HEAT TRANSFER AND FLOW MEASUREMENTS ON A ONE-SCALE GAS TURBINE CAN COMBUSTOR MODEL

Santosh Abraham

Thesis submitted to the faculty of the Virginia Polytechnic Institute and State University in partial fulfillment of the requirements for the degree of

Master of Science

In

Mechanical Engineering

Dr. Srinath V. Ekkad

Dr. Danesh K. Tafti

Dr. Uri Vandsburger

August 29, 2008

Blacksburg, Virginia

Keywords: Combustor liner cooing, Swirler, Infrared Thermal Imaging, Dry Low Emission (DLE) combustors

HEAT TRANSFER AND FLOW MEASUREMENTS ON A ONE-SCALE GAS TURBINE CAN COMBUSTOR MODEL

Santosh Abraham

(ABSTRACT)

Combustion designers have considered back-side impingement cooling as the solution for modern DLE combustors. The idea is to provide more cooling to the deserved local hot spots and reserve unnecessary coolant air from local cold spots. Therefore, if accurate heat load distribution on the liners can be obtained, then an intelligent cooling system can be designed to focus more on the localized hot spots. The goal of this study is to determine the heat transfer and pressure distribution inside a typical can-annular gas turbine combustor. This is one of the first efforts in the public domain to investigate the convective heat load to combustor liner due to swirling flow generated by swirler nozzles. An experimental combustor test model was designed and fitted with a swirler nozzle provided by Solar Turbines Inc. Heat transfer and pressure distribution measurements were carried out along the combustor wall to determine the thermo-fluid dynamic effects inside a combustor. The temperature and heat transfer profile along the length of the combustor liner were determined and a heat transfer peak region was established.

Constant-heat-flux boundary condition was established using two identical surface heaters, and the Infrared Thermal Imaging system was used to capture the real-time steady-state temperature distribution at the combustor liner wall. Analysis on the flow characteristics was

also performed to compare the pressure distributions with the heat transfer results. The experiment was conducted at two different Reynolds numbers (Re 50,000 and Re 80,000), to investigate the effect of Reynolds Number on the heat transfer peak locations and pressure distributions. The results reveal that the heat transfer peak regions at both the Reynolds numbers occur at approximately the same location. The results from this study on a broader scale will help in understanding and predicting swirling flow effects on the local convective heat load to the combustor liner, thereby enabling the combustion engineer to design more effective cooling systems to improve combustor durability and performance.

ACKNOWLEDGEMENTS

I would like to express my sincere gratitude to Dr. Srinath V. Ekkad for his continuous guidance through the course of this thesis. The discussions, encouragement and critiques provided by him were of great essence to the progress of this work. My special thanks to him for his patience and faith in me and also for funding me.

I would also to thank my committee members Dr. Danesh K. Tafti and Dr. Uri Vandsburger for their valuable suggestions. Dr. Tafti and Sunil Patil were instrumental in the CFD validation of the work presented in this thesis. I am also indebted to my fellow lab mates Alok Dhungel and Yap S. Goh at Louisiana State University who guided me through the initial phases of this research. I am also grateful to my colleagues Pritish Parida and Alex Navin for extending their help.

The task of writing this thesis was made a lot easier, thanks to the efforts of Tracy James who spent many sleepless nights making this thesis readable. I would like to express my gratitude to my roommates Cherian Korah and Sebastian Eluvathingal, who have endured me and managed to keep me sane over the past two years.

Finally, I am forever indebted to my parents for their prayers and encouragement over all these years.

TABLE OF CONTENTS

ABSTRACT …….. ii

ACKNOWLEDGEMENTS ……. ……..... iv

LIST OF FIGURES ……. …….. viii

NOMENCLATURE …….. x

CHAPTER 1: INTRODUCTION …….. 1

1.1 Liner Wall Cooling Systems …… 3

1.2 Pollutant Emissions …….. 5

1.3 Solar Dry Low Emission (DLE) Combustor ……... 8

1.4 Focused Cooling ……10

1.5 Swirler …… 12

1.6 Literature Survey ……... 13

1.7 Experimental Objectives …… 15

CHAPTER 2: EXPERIMENTAL APPARATUS ……... 17

2.1 Transient condition experiment setup …… 17

2.2 Steady-State condition experiment setup ……... 18

2.2.1 Inlet air supply …… 18

2.2.2 Swirler …… 19

2.2.3 Combustion Chamber ……. 22

2.2.4 Surface Wall heater ……. 24

2.2.5 Infrared Thermal Imaging System …….. 26

2.2.6 Personal Daq USB Data Acquisition Module ……. 28

2.2.7 NetScanner 9816/98RK Ethernet Intelligent Pressure Scanner …….. 29

CHAPTER 3: EXPERIMENTAL METHODOLOGY ……... 31

3.1 Transient Heat Transfer Measurement ……... 32

3.2 Steady-State Heat Transfer Measurement ……. 35

3.3 Uncertainty Analysis ……. 37

3.3.1 Transient condition experiment uncertainty analysis ……. 37

3.3.2 Steady-State condition experiment uncertainty analysis …… 38

CHAPTER 4: RESULTS ……. 42

4.1 Transient condition experiment: Heat transfer data .....……. 42

4.2 Steady-State condition experiment: Heat transfer data …….……. 44

4.3 Validation with CFD Results ….……..……..... 50

4.4 Effect of Reynolds number on Nusselt number augmentation …….. 51

4.5 Steady-State condition experiment pressure data …….. 51

CHAPTER 5: CONCLUSIONS …….. 53

REFERENCES …… 55

LIST OF FIGURES

Figure 1.1: Typical Combustor Liner Wall Film Cooling [23] ……... 4

Figure 1.2: Influence of Primary-Zone temperature on CO and NOx emissions [1] …….. 7

Figure 1.3: Solar Turbines MARS Low-NOx Combustor [24] ……... 9

Figure 1.4: Focused Cooling [23] …….. 11

Figure 2.1: Transient condition experiment schematic …….. 17

Figure 2.2: Blower with the adjustable frequency AC drive (Photo by Author) ……..…. 19

Figure 2.3: Swirler mounted at the entrance to the combustion chamber (Photo by Author) ... 20

Figure 2.4: 3-D CAD model of the swirler showing the vanes and the fuel injectors ……... 21

Figure 2.5: 3-D CAD model of the Solar Turbines swirler with the casing …….. 22

Figure 2.6: The model combustion chamber with the IR camera windows (Photo by Author) .23

Figure 2.7: The model combustion chamber with pressure taps (Photo by Author)…….. 23

Figure 2.8: Schematic of the Surface Heater [23] ….……. 24

Figure 2.9: Heat loss from the liner wall as a function of temperature ……. 25

Figure 2.10: IR image of the surface heater on the liner wall (Photo by Author) ……..….26

Figure 2.11: FLIR SC640 Infrared Camera (Photo by Author) ...……...……. 27

Figure 2.12: OMB-DAQ-54 Personal Daq (Photo by Author) ……..…….. 29

Figure 2.13: NetScanner multi-channel pressure acquisition system (Photo by Author) …… 30

Figure 3.1: Flow over an infinitely thick plate [23] …….…….. 32

Figure 3.2: Steady-State experiment setup (Photo by Author) ……..…… 35

Figure 4.1: Local Nusselt Number Augmentation with respect to fully developed straight pipe values at Re=50,000 …….. 43

Figure 4.2: 2-D temperature distribution (in °C) along length and width of the liner wall for Re=50,000and Re=80,000 ……... 44

Figure 4.3: 2-D heat transfer distribution (in W/m^2K) along the liner wall for Re=50,000 and Re=80,000 ……. 45

Figure 4.4: 1-D heat transfer coefficient distribution along the liner wall for Re=50,000 and Re=80,000 ……. 46

Figure 4.5: Nusselt number variations with reference to combustor diameter for both Re=50,000 and Re=80,000 …….. 47

Figure 4.6: Local Nusselt Number Augmentation with respect to fully developed straight pipe values at Re=50,000 and Re=80,000 ……. 48

Figure 4.7: Comparison of Local Nusselt Number Distribution to FDF Straight-pipe Estimation for Re=500,000 and 662,000 [23] ……... 49

Figure 4.8: Nusselt number Augmentation for Re = 50000 ……...….... 50

Figure 4.9: Variation of Peak Nusselt number augmentation with Reynolds number ……... 51

Figure 4.10: Pressure distribution along the liner wall …….... 52

NOMENCLATURE

S_N Swirl number

G_m Axial flux of angular momentum

G_t Axial thrust

D_{sw} Outer swirler diameter

Nu Nusselt number

h Convective heat transfer coefficient

ρ Density of the fluid

U Mean fluid velocity

μ (absolute) dynamic fluid viscosity

Re_D Reynolds number

k Thermal conductivity of air

T_w Combustor liner wall temperature

T_i Combustor liner initial temperature

T_m Mainstream air temperature

α Thermal diffusivity of the wall

t Time span for which the measurements were taken

Q Heat generation

V Electrical voltage

R Electrical Resistance

Pr Prandtl Number

P_s Static Pressure

P_{in} Inlet Static Pressure

CHAPTER 1: INTRODUCTION

Gas turbine engines have proven to be an effective means of converting fuel into usable power either through direct shaft power, or thrust produced from the high momentum exhaust gases. At the end of World War II, a search was on for effective high output propulsion systems to power the airplane which was regarded as the greatest addition to military warfare. The first few gas turbine engines were aimed only at performance, without taking into consideration efficiency or emissions. As the years went by, there arose new arenas for gas turbines: commercial air travel and industrial power generation. Efficiency, reliability and emission considerations came into the forefront.

The fundamental thermodynamic principles that make gas turbine engines feasible are based on the properties of the working fluid. The working fluid, air, is compressed and then heated with the addition and burning of fuel. The energy that is released from the air expanding through the turbine is more than the energy that is required to compress the air. This energy acquired is amplified by compressing the fluid to higher pressures and by increasing the temperature at the turbine inlet. The temperatures will therefore reach near or over the failure point of the turbine materials, necessitating extensive cooling of the parts exposed to the hot flow. The coolant air is extracted from the compressor section before it reaches the combustion chamber. It is sent to the parts of the engine that are in the hot gas path, i.e. combustor liner and the turbine blades, which need to be cooled using innovative designs.

In order to obtain higher efficiency, the firing temperatures are raised and to achieve the stringent emissions levels it is required to maintain the combustion zone temperatures as low as possible. The desire for higher efficiency and the requirement for lower emissions have reduced

the amount of cooling air that the combustion engineer has available for cooling of the combustor liner, as more air is utilized in the premixing process and reaction zones to maintain temperatures as low as possible. Due to this the effectiveness of backside cooling techniques becomes more critical.

This study focuses on the interaction between the hot swirling gases and the liner wall within a gas turbine combustor. Better understanding of the heat transfer process from the gases to the combustor liner is essential so that effective usage of the available coolant air may be planned.

1.1 Liner Wall Cooling Systems

The liner contains the combustion process and facilitates the distribution of air to all the various zones in the combustor in the prescribed amounts. It is essential that the liner must be structurally strong to withstand the buckling load created by the pressure differential across the liner wall. It must also have sufficient thermal resistance to withstand continuous and cyclic high temperature operation. This is accomplished by the use of high temperature, oxidant resistant materials combined with the effective use of cooling air. Nowadays, many combustors use up to 40% of the total combustor air-mass flow in liner wall cooling. The problem of liner wall cooling has become more severe with increasing engine pressure ratio which is accompanied by increasing inlet air temperature, which results in higher flame temperature, which, in turn increases the heat transfer to the liner wall. The higher inlet temperature also reduces the effectiveness of the coolant air. Increasing the amount of air used for film cooling would worsen the radial temperature profile at the combustor outlet, thereby reducing the life of the turbine blades and also leading to higher pollutant emissions. Thus, there is a need to make more efficient use of the available cooling air [1].

Present day technology and techniques are capable of pushing the thermal efficiency higher than ever and increasing the engine power output with better control of air-fuel ratio (AFR) and flame temperatures. With increase in the thermal efficiency and power output, turbine inlet temperature will also increase consequently from 1700K to 2200K, which is higher than the blade material melting temperature at around 1850K. To overcome this, various solutions have been tried and tested; using thermal barrier ceramic coating (TBC) and other cooling techniques such as film cooling, back-side cooling, jet impingement cooling, etc. to remove as much heat load as possible from engine components and allow for longer durability of components.

However, excess removal of heat from gas turbines is unfavorable as it will reduce the thermal efficiency because the heat generated is the required energy. Therefore a proper design of cooling system is important to compensate for both thermal efficiency and destructive heat loads.

Film cooling technique has been used as the most popular cooling system over the past few decades. Figure 1.1 shows the typical film cooling system used in conventional turbine combustor. Here, the secondary coolant air is injected through holes or slots into the mainstream air flow in the combustion chamber to form a thin separate coolant air film or jacket which prevents the mainstream hot air from direct contact with the combustor liner walls. This leads to lower flame temperature and higher liner pressure drop which promotes better mixing.

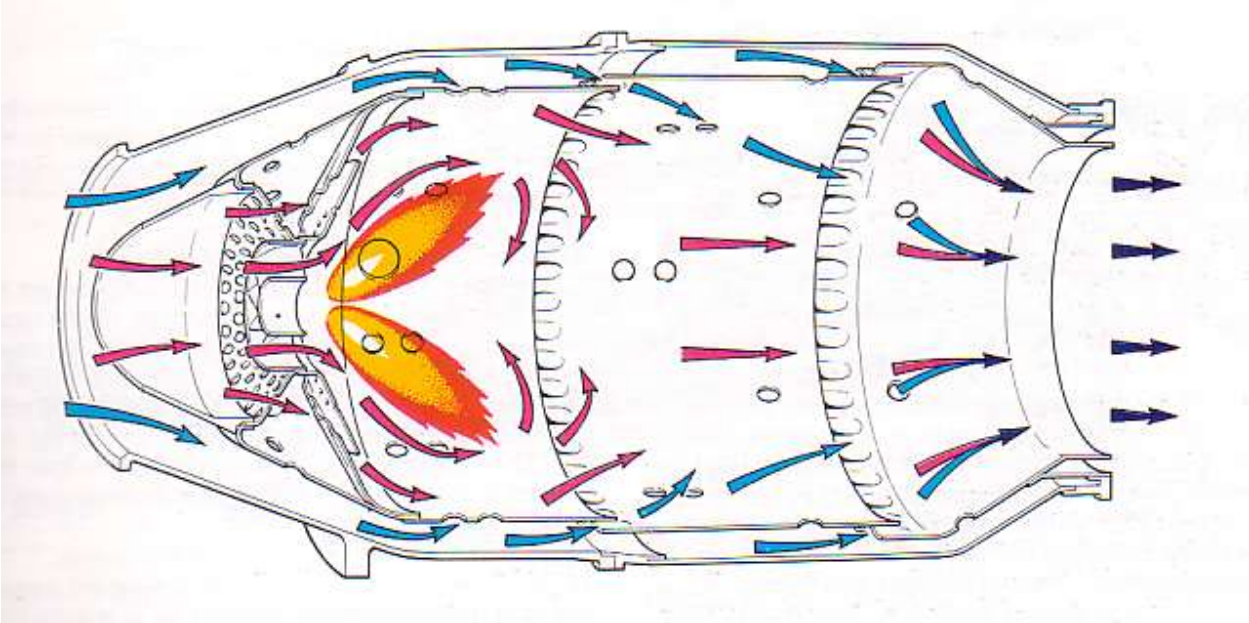

Figure 1.1: Typical Combustor Liner Wall Film Cooling [23]

The main drawback with film cooling is that the secondary coolant air stream will alter the air fuel ratio by mixing itself with the mainstream air flow. It also causes a non-uniform radial temperature distribution and premature failure of materials due to thermal stresses.

Furthermore, the amount of liner wall cooling air added into the primary zone will significantly enhance Carbon Monoxide (CO) emissions. At the near wall region where the wall cooling air is employed, the temperature of air gets relatively low such that all chemical reactions cannot be possible resulting in unburned hydrocarbons. At the same time the temperature of air at the center core of the primary zone will get so high that it results in higher NOx emissions. These hot regions can generate 25-30 ppm NOx and the relatively cooler regions near the liner results in higher CO in the exhaust. Thus, even when the overall combustion zone is maintained below the NOx formation threshold temperature range (1500-1650°C), the NOx levels will still be affected due to the center core region (as shown in Figure 1.2). Therefore we have an undesirable situation with the worst overall combined emissions levels of both CO and NOx. This has led to a lot of research intended to improve the temperature uniformity within the combustion primary zone.

1.2 Pollutant Emissions

Pollutant emissions from combustion processes have become of great public concern due to their impact on health and the environment. There has been great progress over the past decade in civil aviation, now perceived as one of the world's fastest growing energy-use sectors and also in stationary gas turbines, the prime movers in the gas and oil industry and extensively used in power generation. These developments have led to an urgent call to reduce pollutant emissions from all types of gas turbines [1].

Pollutant emissions from combustion processes have aroused public attention due to their unfavorable effect on health and environment. The environmental regulations governing pollutant emissions have become increasingly stringent, thereby forcing combustion engineers to

improve cooling techniques that reduce gas turbine emissions levels of NOx, carbon monoxide, and unburned hydrocarbons. Therefore, pollutant emission control becomes an essential factor to be considered during the design of an effective cooling system.

During the last three decades, the United States Congress enacted a series of Clean Air Acts which significantly strengthened regulation of air pollution. These Acts set numerical limits on the concentrations of a basic group of air pollutants and provide reporting and enforcement mechanisms. In 1999, the United States EPA replaced the Pollution Standards Index (PSI) with the Air Quality Index (AQI) to incorporate new 993PM2.5 (PM2.5 refers to particulate matter that is 2.5 micrometers or smaller in size) and Ozone standards.

The present Environmental Protection Agency (EPA) regulations have made more stringent emissions standards for NOx limits. The fact that NOx emission level depends exponentially on flame temperature has been studied and proved. Inlet air temperature, residence time in the primary zone, equivalence ratio, and combustion pressure might also affect NOx emissions production level. However, primary-zone flame temperature is still regarded as the most significant contributor to NOx emissions issues. Therefore in order to reduce NOx emissions, it is vital that the flame reaction temperature is lowered and localized hot spots from the combustion reaction zone are eliminated. The residence time for the formation of NOx should also be minimized. However, lowering the flame temperature encourages the formation of Carbon Monoxide and unburned Hydrocarbons. Figure 1.2 illustrates how the formation of CO and UHC increases at lower temperatures, which is at low-power conditions, and decreases, with an increase in power as opposed to NOx and smoke, which are relatively insignificant at low power conditions and higher at high-power conditions.

The primary zone flame temperature for most conventional combustors ranges from 1000K at low power condition to 2500K at high power conditions. Figure 1.2 shows that when the combustion temperature is below 1670K, CO and UHC are formed appreciably due to incomplete combustion from the lack of adequate oxygen and also due to the dissociation of 2 *CO*; whereas at temperatures higher than 1900K, excessive amounts of NOx are produced. This essentially leaves us with a narrow band of temperature range between 1670K and 1900K where the CO and NOx emissions levels are within tolerable limits.

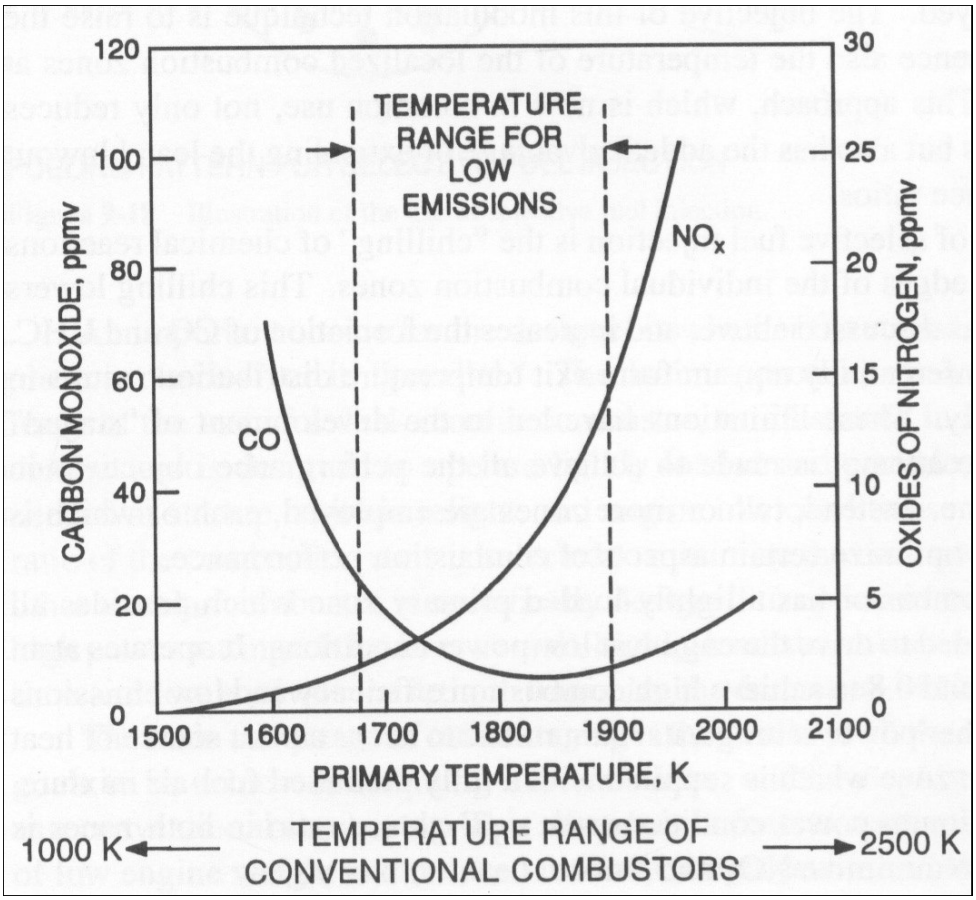

Figure 1.2: Influence of Primary-Zone temperature on CO and NOx emissions [1]

The second vital reason for controlling flame temperature is to obtain uniformity of local temperature distribution. Even though the overall averaged flame temperature is properly

controlled within the desirable temperature range between 1670K and 1900K, there are going to exist localized hot and cold spots that can result in the local temperatures in separate regions within combustion zone to rise higher than 1900K, escalating NOx emissions, and to drop lower than 1670K increasing CO and UHC. This defeats the purpose of narrow band flame temperature control and seriously affects the pollutant emissions. One effective way of better controlling both the flame temperature and AFR, is to use less liner wall-cooling air, especially in the primary zone. This will not only reduce local non-uniformity but also provide more accurate prediction and better control to mainstream flow temperature. Due to this requirement, the effectiveness of backside cooling techniques involving impingement, convection, or surface enhancement techniques becomes more critical. Due to longer operating cycles for power turbines, combustor liner needs to meet durability targets of 30000 hours. To avoid liner failure from over-temperature, it is extremely important to quantify the liner heat load accurately in the lean premixed combustor environment. This means that cooling techniques for the low NOx combustor liner requires more backside cooling and less or almost no film cooling [2].

1.3 Solar Dry Low Emission (DLE) Combustor

Two of the major performance criteria in the design of dry low-NO_x combustors for stationary gas turbines are

1) Meeting the emissions requirements and controlling the variation of emissions levels across the load range of the engine.

2) To achieve stable combustion at all operating conditions, superior system response to rapid load changes and acceptable levels of combustion.

Solar Turbines is among the pioneers in the development of dry low-emissions combustors for industrial gas turbines [1].

The DLE combustors utilize premix gaseous fuel lean-burn combustion active control technique, which stages injection of the fuel-air mixture to carefully control the location and the sequence of delivery within the combustion chamber. DLE combustors do not use water or steam injection into the main chamber. In order to efficiently maintain the combustion flame temperature at a favorable AFR within a narrow band of operating flame temperatures (1500~1650°C) which gives the lowest overall production level of NOx, CO, and UHC emissions, DLE combustors implement a complex array of proprietary fuel-air-nozzles and combustion system geometry. Figure 1.3 shows an example of modern dry low NOx emission combustor used in Solar MARS engines designed by Solar Turbines.

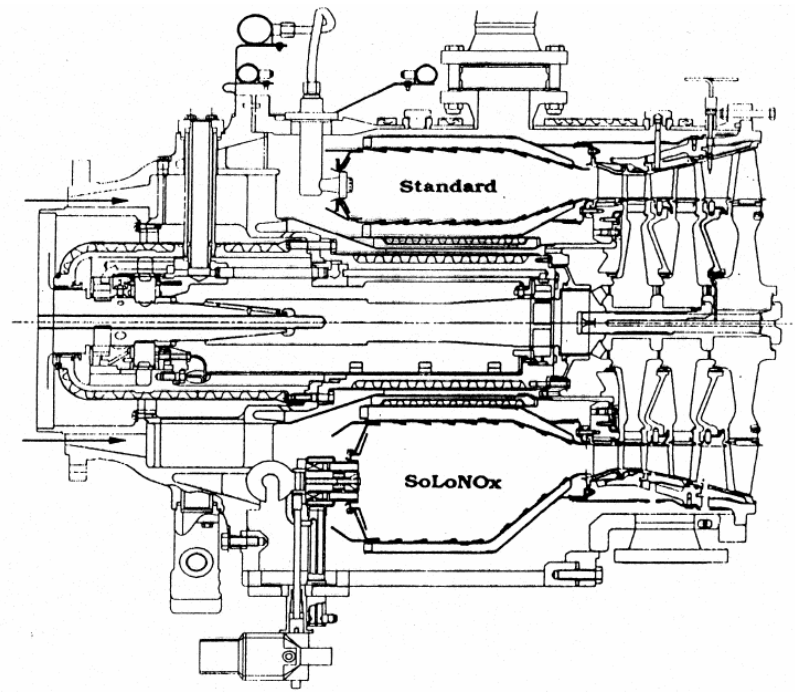

Figure 1.3: Solar Turbines MARS Low-NOx Combustor [24]

The new DLE combustor regulates the combustor airflow and pilot fuel flow over the entire engine-operating map. The need to control these parameters has further complicated the

control system design compared to that of a conventional gas turbine. Below 50% load, the combustor airflow is managed similar to that of a conventional engine. Above 50% rated load, Solar's DLE engine enters the "low emissions mode," altering either the bleed valves or inlet guide vanes to keep the combustion primary zone temperature within a particular range. Solar's DLE gas turbine controls utilize the turbine inlet temperature as a reference of the primary zone temperature in order to control the bleed valve or inlet guide vane position as a function of turbine load [3].

1.4 Focused Cooling

To achieve present day stringent emission levels it is necessary to maintain the combustion zone temperatures within allowable limits. This essentially requires more air to be utilized in the premixing process and reaction zones. This means that the combustor liner is to be cooled without the use of cooling air bleed as hot-side film cooling. Therefore cooling must be achieved through back-side convective methods alone. During the years various methods for the cooling of combustor liners have been tried and tested. In order to ensure system durability and long life, combustor liner cooling must be predictable and reliable [4].

Due to the above mentioned reasons, modern DLE combustor liners are designed to operate with minimum usage of film cooling. Complete cooling across the combustor length is just not practical, as the amount of cooling air available is limited. However, with data revealing the accurate heat load distribution on the liners, an intelligent cooling system can be designed, which focuses more of the coolant air onto the localized hot spots and prevent unnecessary coolant air from reaching the relatively cooler areas. Therefore, a highly efficient cooling system with focused cooling configurations plays a critical role in improving the efficiency of gas

turbine engines and meeting the pollution emissions requirements. Solar Turbines, in their effort to reduce emissions, have introduced the Augmented Backside-Cooled (ABC) liner. Here the cooling air does not mix with the combusting mixture in the combustor primary zone. This eliminates a significant amount of quenching, which inherently lowers the CO emissions. This design also allows the combustor to be designed for a cooler flame that reduces NO_x emissions.

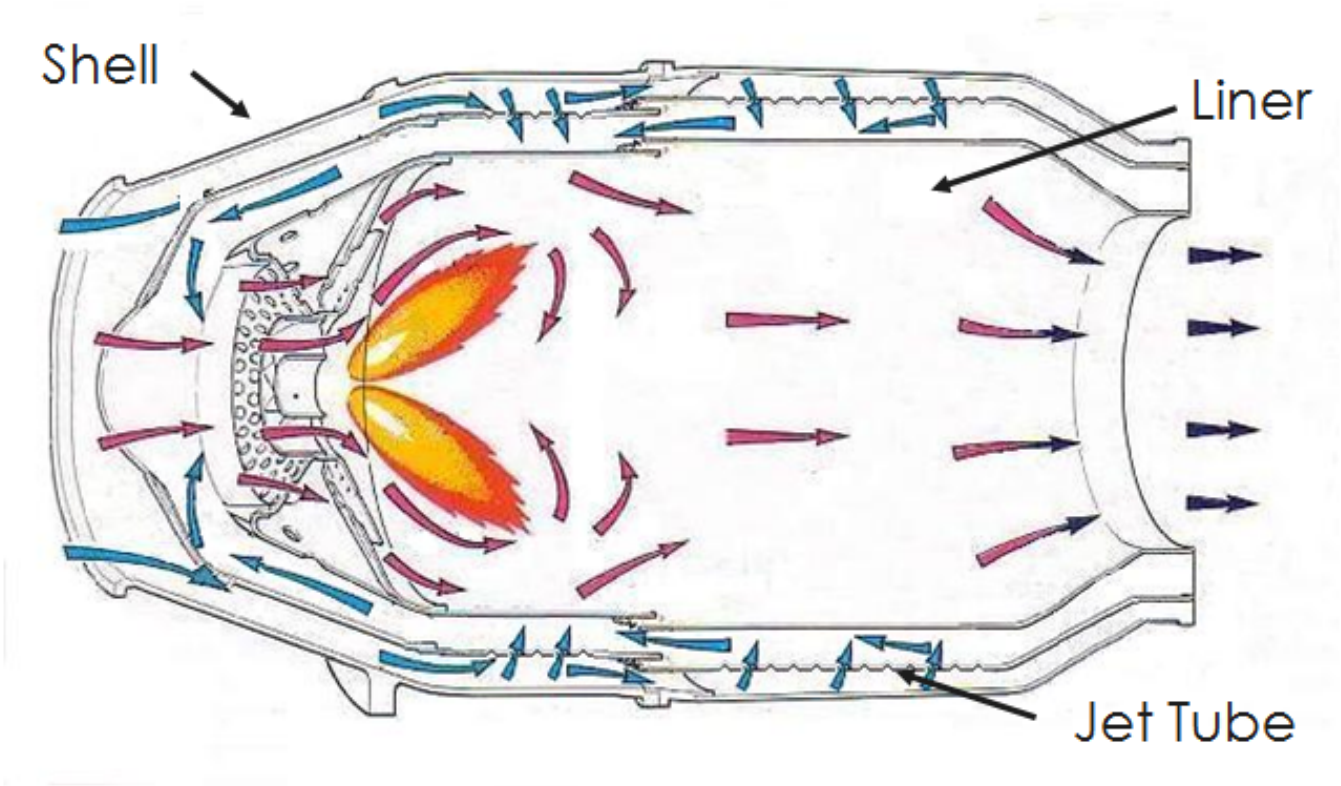

Figure 1.4: Focused Cooling [23]

1.5 Swirler

The primary zone airflow pattern is an important factor in flame stability. One of the common features among all the different types of airflow patterns employed is the creation of a toroidal flow reversal that entrains and recirculates a fraction of the hot combustion products to mix with the incoming air and fuel. These vortices are continually refreshed by air admitted through holes pierced in the liner walls, supplemented in most cases by air flowing through swirlers and flare-cooling slots, and by air employed in atomization. An effective way of inducing flow recirculation in the primary zone is by putting in a swirler in the dome around the fuel injector. Vortex breakdown arising by the swirling flow causes recirculation in the core region when the amount of rotation imparted to the flow is high. The swirl components produce strong shear regions, high turbulence and rapid mixing rates. These characteristics of swirling flows have been used to control the stability and intensity of combustion and the size and shape of the flame region [1].

Air swirlers are widely used in both tubular and annular combustors. The two main types of swirlers are axial and radial. They are often fitted as single swirlers, but are also sometimes mounted concentrically providing either co-rotating or counter-rotating airflows. These swirlers can be fitted with flat vanes or curved vanes. The flow fields generated by both the axial and the radial swirlers are approximately the same. Beer and Chigier [5] proposed the usage of Swirl Number, a non-dimensional parameter to characterize the amount of rotation imparted to the axial flow [1]:

$S_N = 2\ G_m / (D_{sw} G_t)$

Where G_m = axial flux of angular momentum

G_t = axial thrust

D_{sw} = outer swirler diameter

If swirl number is less than around 0.4, no flow recirculation is obtained and the swirl is therefore described as weak. Most swirlers operate under strong swirl conditions. For swirl number greater than 0.6, the swirl is described as strong. The primary function of the swirler is to induce combustion products to flow upstream to meet and merge with the incoming fuel and air. For weak swirl there is hardly any flow recirculation, but when the swirl number is increased and reaches a critical value ($S_N > 0.4$), the static pressure in the central core just downstream of the swirler becomes low, thereby creating flow recirculation. Kilik [6] carried out velocity measurements along the swirler axis for several swirler designs and established the influence of key geometric parameters on the reverse mass flow rate. His results showed that the curved-vane swirlers induce larger reverse mass flow rate. Kilik also studied the separate effects on recirculation zone-size. His experimental data show that the size of the recirculation zone is increased by increasing the vane angle, increasing the number of vanes, decreasing the vane aspect ratio and changing from flat to curved vanes.

1.6 Literature Survey

Older gas turbine engines used combustion dilution air and film cooling of various types as a solution to the cooling problems in combustor liners. Several studies have been conducted by Chin et al [7], Metzger et al. [8], Andrews et al. [9] and Fric et al. [10]. Schulz [11] presented a first-rate review of combustor cooling by film cooling methods as well as combined film and convective cooling methods.

Ferrara et al. [12] studied convective and film cooled combustor analysis and developed an analysis tool including impingement, turbulated and film cooling methods. Smith and Fahme [13] focused on liner designs without film cooling for low emission combustors dealing with rib turbulated channel type flow cooling. Bailey et al. [4] conducted experiments and numerical simulations to understand the heat transfer characteristics of a stationary gas turbine combustor liner cooled by impingement jets and cross flow between the liner and sleeve.

Several articles that focus on the development of DLE combustors for industrial gas turbine engines have been published. Studies by Smith et al. [14, 15, and 16], Vandervort et al. [17], White et al. [18] and Roberts et al. [19] have focused on development of low NOx combustors with the viewpoint of producing lower emissions. Although the designs of these combustors vary, all of them use minimal film cooling. Arellano et al. [20] presented a study on an effective backside cooling scheme for an ultra-lean premixed combustion system. The augmented backside cooled liner, in their study, eliminates film cooling in the combustor primary zone and uses trip strip turbulators along the cold side of the liner to enhance heat transfer and thermal barrier coatings on the gas side liner wall to reduce heat load. Behrendt et al. [21] recently designed a test rig for the characterization of advanced combustor cooling concepts for gas turbine combustors. The test rig is intended to allow investigations at elevated pressures and temperatures representing realistic operating conditions of future low emission combustors. Lu et al. [22] recently studied the effect of different swirl angles for a Dry Low Emission combustor on flow and heat transfer distributions.

In an effort to achieve a fuel lean mixture, the fraction of the cooling air has to be reduced from up to 50% of the combustor air in conventional combustors to less than 30 percent in lean combustors. Hence, novel combustor cooling concepts have to be developed, which

makes possible this reduction of cooling air. Even with present day advanced CFD capabilities, experimental analysis plays a crucial role in the understanding and development of combustor cooling technology. There are no published studies on experimental measurement of heat transfer distributions on the gas side liner surface.

1.7 Experimental Objectives

It is clear that compared to conventional combustors, "Dry Low Emission" combustors are a better solution for compromise between emissions level and performance. The goal is to minimize film cooling and ensure that back-side wall cooling is capable of cooling the combustor wall acceptably and adequately. Due to the fact that the available coolant air is limited, focused cooling approach is required to properly allocate the cooling supply based on the local demand within a combustor. Thus, it is imperative that the actual heat load distribution on the liner walls at different flow conditions is established.

The combustor model is fitted at its inlet with a typical swirler for a can combustor provided by Solar Turbines Inc. This study is an effort to investigate the effect of flow through a high-angle swirler nozzle on the convective heat load of a combustor liner. The objectives of this study are to experimentally measure the heat transfer distribution on the liner wall in an effort to determine the locations of higher heat load. The pressure distribution along the combustor liner walls was also measured. Similarity analysis is an important step in these experiments, since they are not conducted at actual engine conditions, but at conditions suitable for accurate testing. Dimensionless parameters are used in similarity analysis in order to relate the low temperature

results to engine conditions. Two important dimensionless parameters used in this study are Nusselt number and Reynolds number.

Nusselt number: $Nu = \frac{hD}{K} = \frac{q"(convective)}{q"(conductive)}$

Where, h = convective heat transfer coefficient

D = characteristic length

K = thermal conductivity of the fluid

The Nusselt number is a dimensionless number and is defined as the ratio of convection heat transfer to conduction heat transfer, where the heat conduction is under the same condition as the heat convection.

Reynolds number: $Re_D = \frac{\frac{\rho U^2}{D}}{\frac{\mu U}{D^2}} = \frac{inertial\ forces}{viscous\ forces}$

Where, ρ = density of the fluid

U = mean fluid velocity

D = characteristic length

μ = (absolute) dynamic fluid viscosity

In fluid mechanics and aerodynamics, the Reynolds number is the ratio of inertial forces to viscous forces and it quantifies the relative importance of these two types of forces for given flow conditions.

CHAPTER 2: EXPERIMENTAL APPARATUS

2.1: Transient condition experiment setup

The experimental setup consists of highly compressed air at over 200 psi sent into a pneumatic valve, which is programmed to maintain the pressure in the combustor region at 3.5% above atmospheric pressure. After the air passes through the pneumatic valve, it flows through the diffuser and then into an 8 inch diameter pipe at the end of which is mounted the swirler. The air then flows into the model combustor chamber, where the IR camera captures images of temperature distribution at six different locations along the combustion chamber.

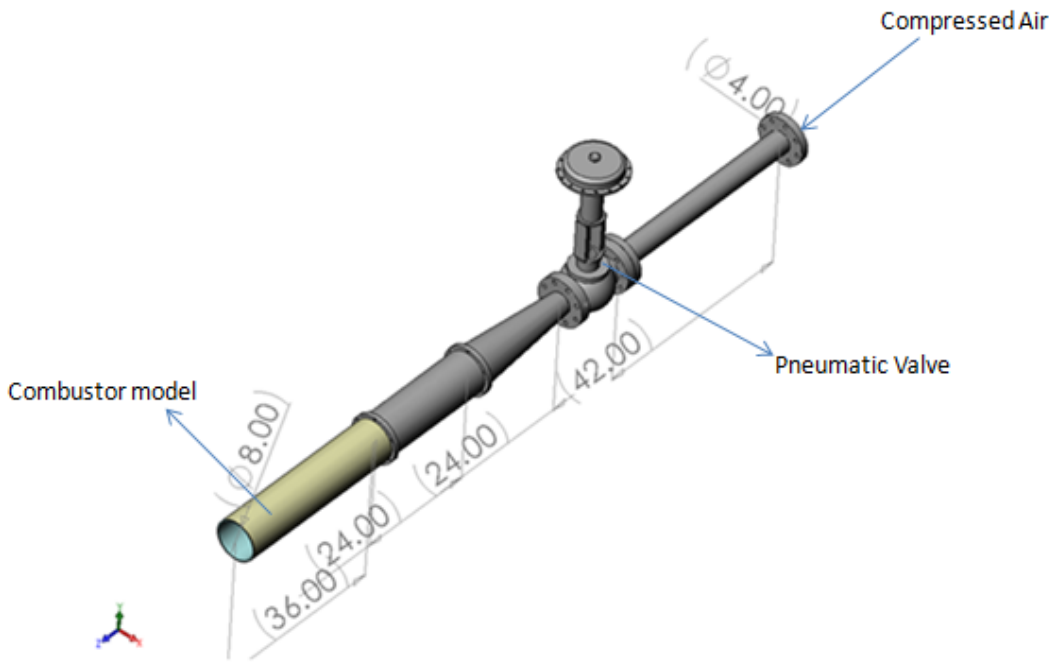

Figure 2.1: Transient condition experiment schematic (dimensions in inches)

(Drawn by Author, 2008)

A resistance surface heater was used to simulate the constant initial temperature boundary condition. Infrared Thermal Imaging system was used to capture the real-time transient temperature distribution on the combustor liner wall. Thermocouples were used to calibrate the IR camera. The thermal images from the camera were post processed using MATLAB to obtain the heat transfer coefficient values using the semi-infinite model assumption. The transient condition experiment was conducted at Louisiana State University.

2.2 Steady-State condition experiment setup

The steady-state condition experiment was conducted at the lab facilities at Virginia Polytechnic Institute and State University. The air supply is provided by a pressure blower whose motor is controlled by an adjustable frequency drive to obtain the required flow rate. The air passes into the combustor chamber through the swirler fitted at its entry. Similar to the transient experiment, an IR camera is used to capture the heat load on the combustor liner wall which is heated using two resistance surface heaters. Thermocouples are placed at required positions to obtain the inlet temperature and to calibrate the IR camera. Pressure distribution along the combustor liner wall was also obtained using a 48 channel Pressure Scanner. A pitot probe is positioned prior to the swirler to obtain accurate values of the velocity of air.

2.2.1 Inlet air supply

The inlet air supply is provided by a 3000 CFM pressure blower from New York Blower Company. An adjustable frequency AC drive (Allen-Bradley PowerFlex 70), which is a variable

speed motor controller that allows precise adjustment of fan speed frequency with a dial pad control panel, was used to control the flow into the combustor chamber. In order to understand the effect of varying speeds, measurements were obtained at two Reynolds numbers (~50,000 and ~80,000), which corresponds to 29Hz and 46Hz fan speed frequency respectively. Figure 2.2 shows the setup of the blower and the variable speed drive.

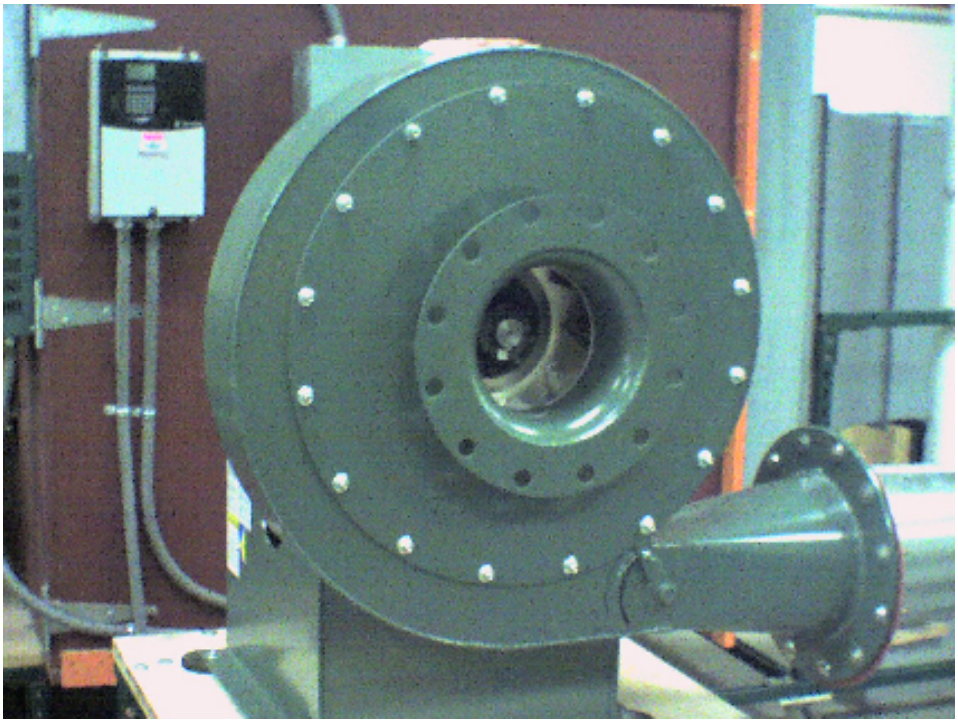

Figure 2.2 Blower with the adjustable frequency AC drive (Photo by Author)

2.2.2 Swirler

From the blower the air flows into the combustor chamber through a 20-vane axial flow swirler retrofitted at the entrance of the chamber. The swirler is used to impart high degree rotation of flow at combustor primary zone which helps to promote better air-fuel mixing and to induce a recirculatory flow in the primary zone. Figure 2.3 shows the swirler setup mounted concentrically at the inlet of the main combustion chamber.

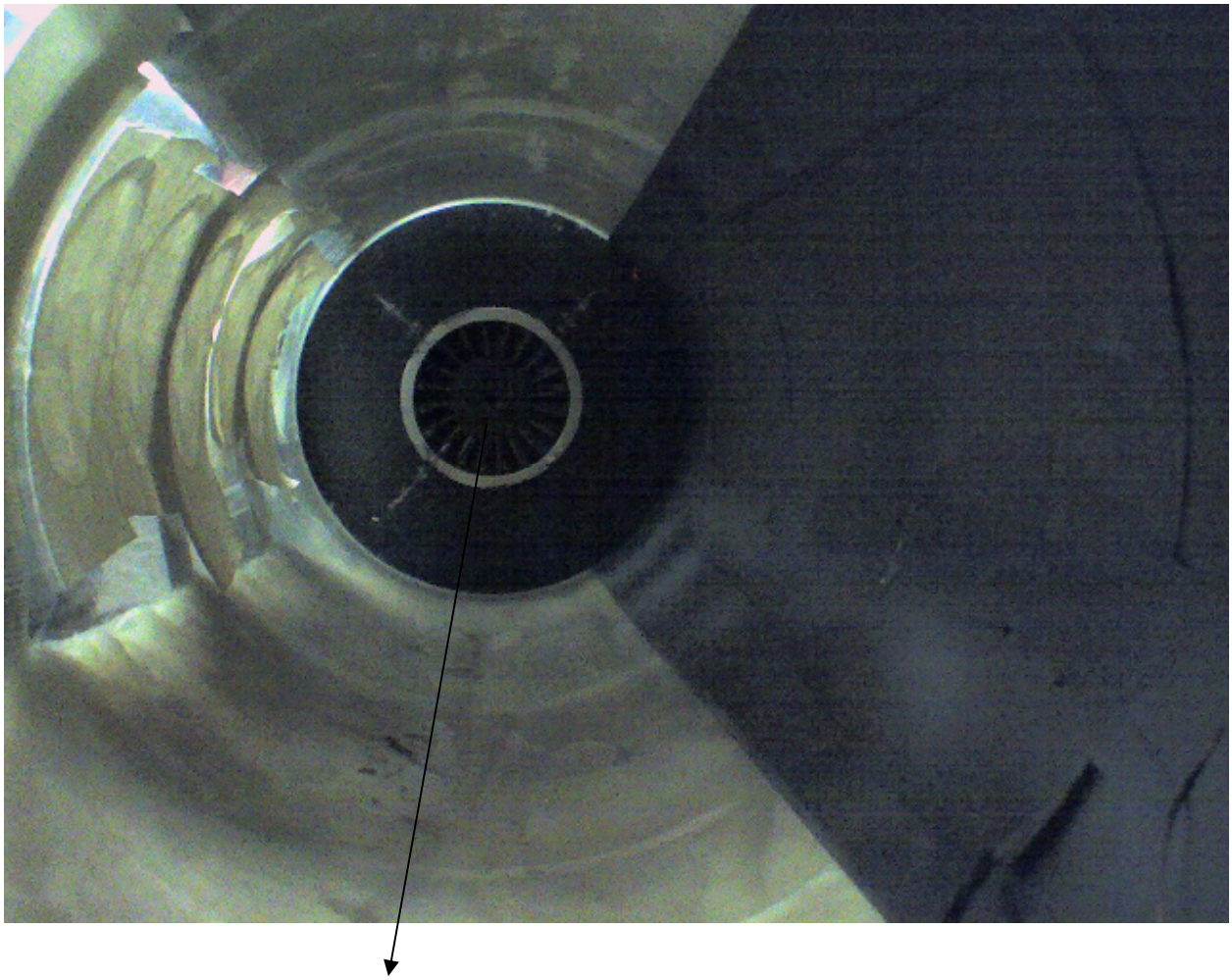

Figure 2.3: Swirler mounted at the entrance to the combustion chamber (Photo by Author)

Figures 2.4 and 2.5 show the 3-D solid model of the swirler that was created using UGS NX CAD software. The inlet vane angle was oriented at zero degree from axial plane and the Swirl angle is 45. The approximate "Theoretical" Swirl number is = 2/3 tan (45) ~ 0.667 [1]. During the real lean-burn engine operation, gaseous fuel is injected from a series of fuel nozzles mounted on bluff bodies to premix with main stream intake air. The premixed gaseous fuel-air mixture is then ignited and the flame is stabilized at the recirculation zone behind bluff bodies. Due to the wakes or recirculation vortices, which are caused by turbulent flow boundary layer

separation on the surface of the bluff body, the flow will be transitioned to highly turbulent so as to provide more energy to the flow and also to help in better air-fuel mixing quality. Furthermore, the recirculation zone behind the bluff body serves as a flame stabilizer to help trap the flame at high speed flow condition. Figure 2.4 illustrates the positioning of the swirler vanes and the bluff bodies in the swirler provided by Solar Turbines.

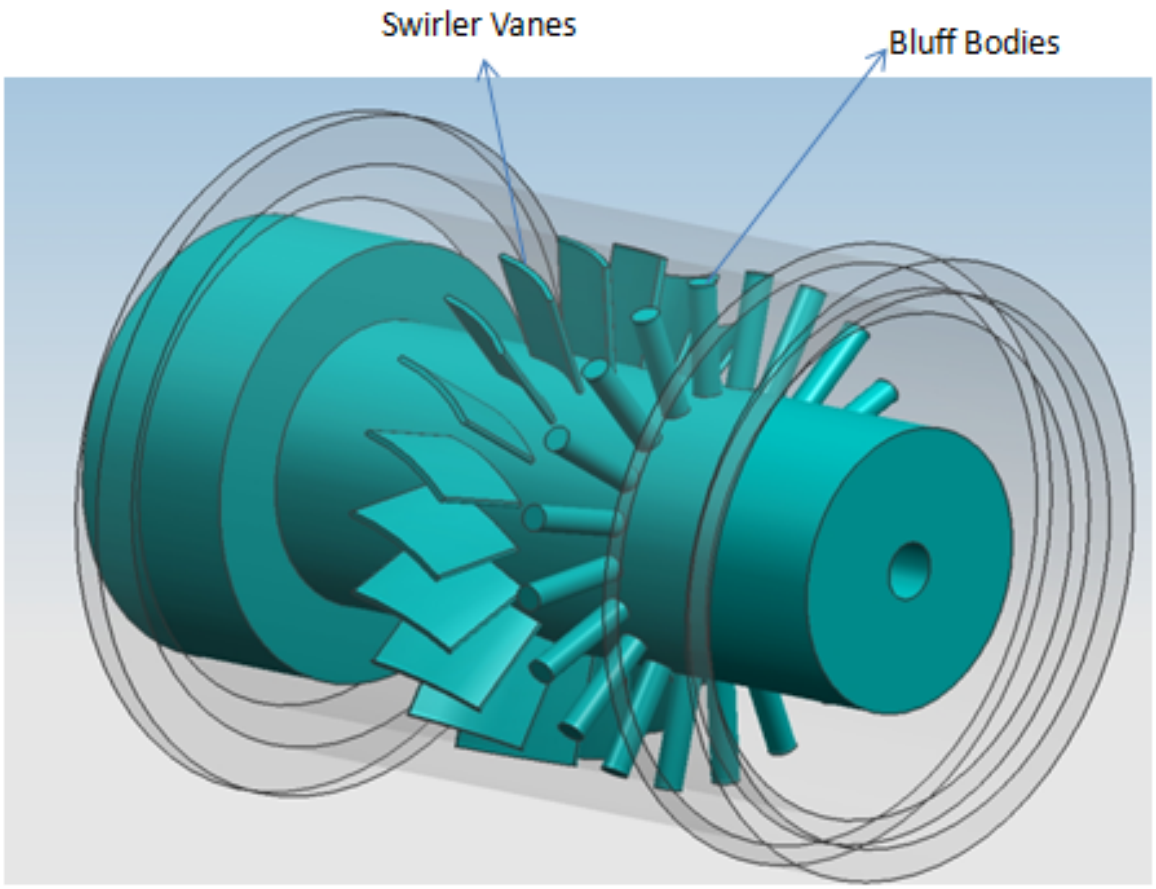

Fig 2.4: 3-D CAD model of the swirler showing the vanes and the fuel injectors (drawn by Author, 2008)

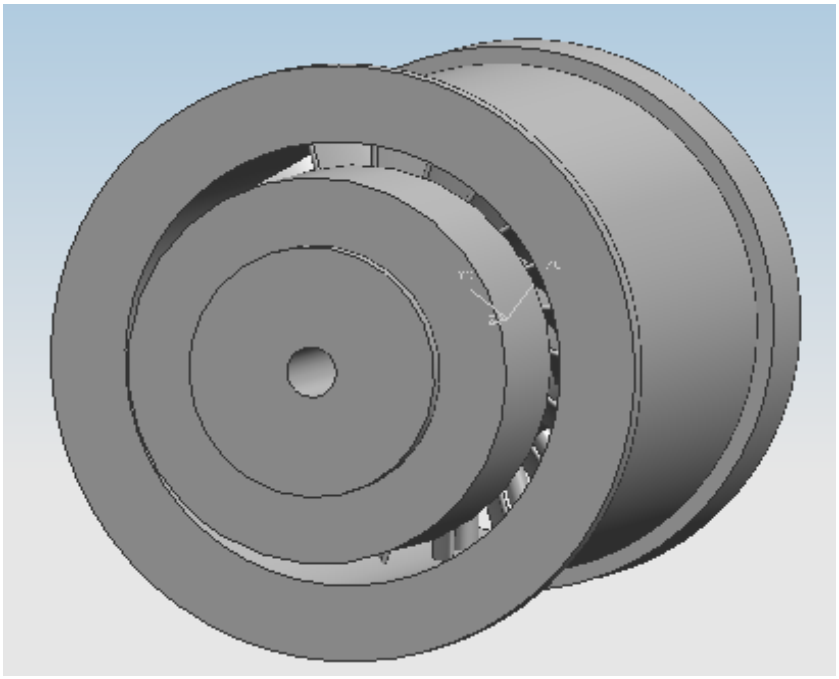

Fig 2.5: 3-D CAD model of the Solar Turbines swirler with the casing (drawn by Author, 2008)

2.2.3 Combustion Chamber

The air is channeled into the combustor chamber through the swirler. The combustion chamber section was fabricated using acrylic material in order to facilitate visibility. Windows for positioning the IR camera lens were cut with equal spacing at six different locations along the main combustion chamber for heat transfer experiments as shown in Figure 2.6. Diametrically opposite to these windows, a surface heater assembly was mounted along the combustor wall. The entire combustion chamber was then covered with insulating material to prevent heat loss. Each of the unused IR camera window holes were sealed during tests. In order to establish the pressure distribution along the liner wall, the combustor chamber was replaced by another one with 96 pressure taps drilled along the liner wall length as shown in Figure 2.7. A pitot probe was inserted prior to the chamber to measure the incoming air velocity into the swirler.

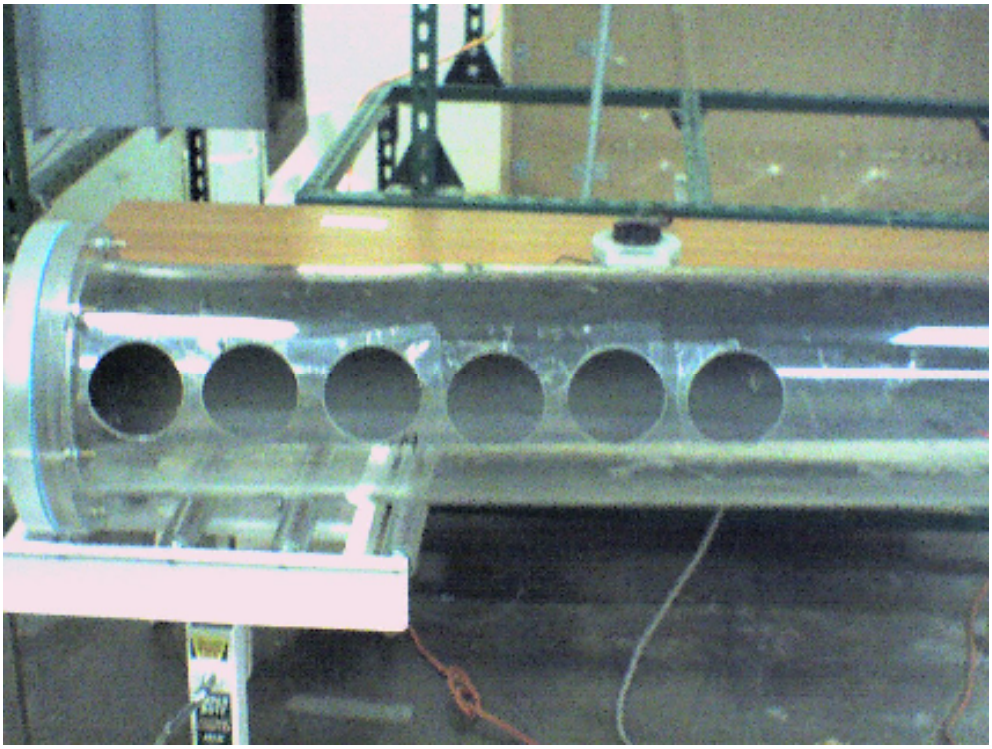

Figure 2.6: The model combustion chamber with the IR camera windows (Photo by Author)

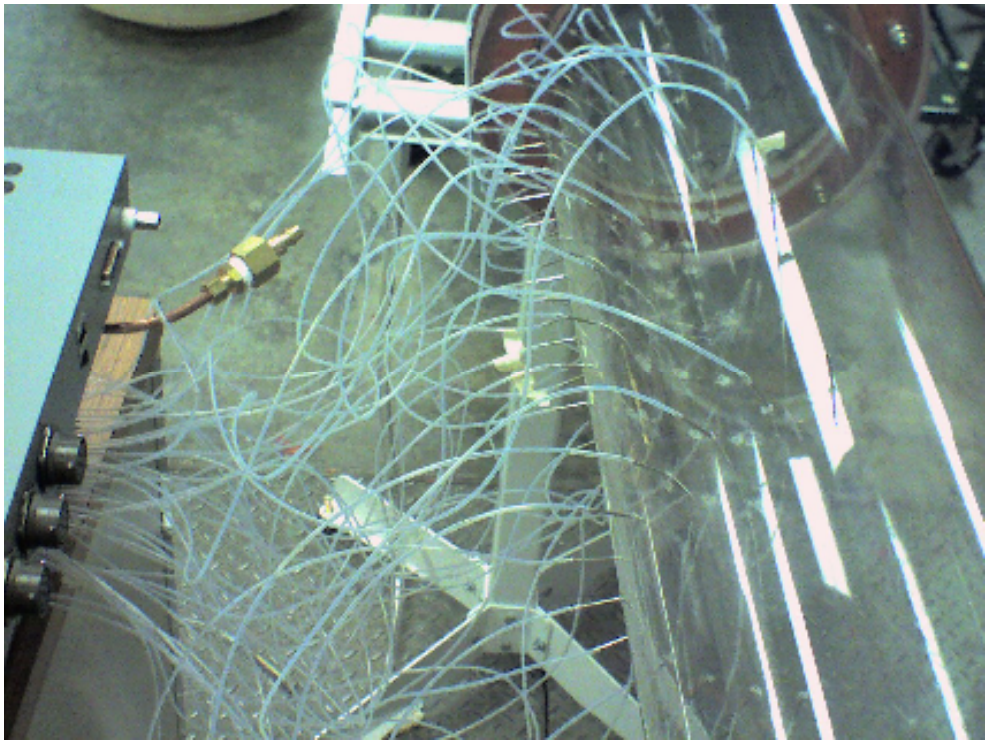

Figure 2.7: The model combustion chamber with pressure taps (Photo by Author)

2.2.4 Surface Wall heater

In order to simulate constant heat flux boundary conditions at the liner wall, the combustor wall diametrically opposite the IR windows was fitted with 2 surface heaters from Minco that cover 0 to 32 inches length from the combustor inlet. Figure 2.8 shows the schematic of the surface heater system construction and the energy processes involved in the steady-state experiment. The face of the heater exposed to the IR camera inside the combustor is coated with thin flat black paint for emissivity purposes. In general, the duller and blacker a material is, the closer its emissivity is to 1. The more reflective a material is, the lower its emissivity. The accuracy of the IR camera is better if the emissivity settings are higher. The other face of the heater is glued onto the acrylic combustor wall. Heat generated from the heater can be adjusted through the use of transformers by varying the voltage and amperage to obtain the required power output.

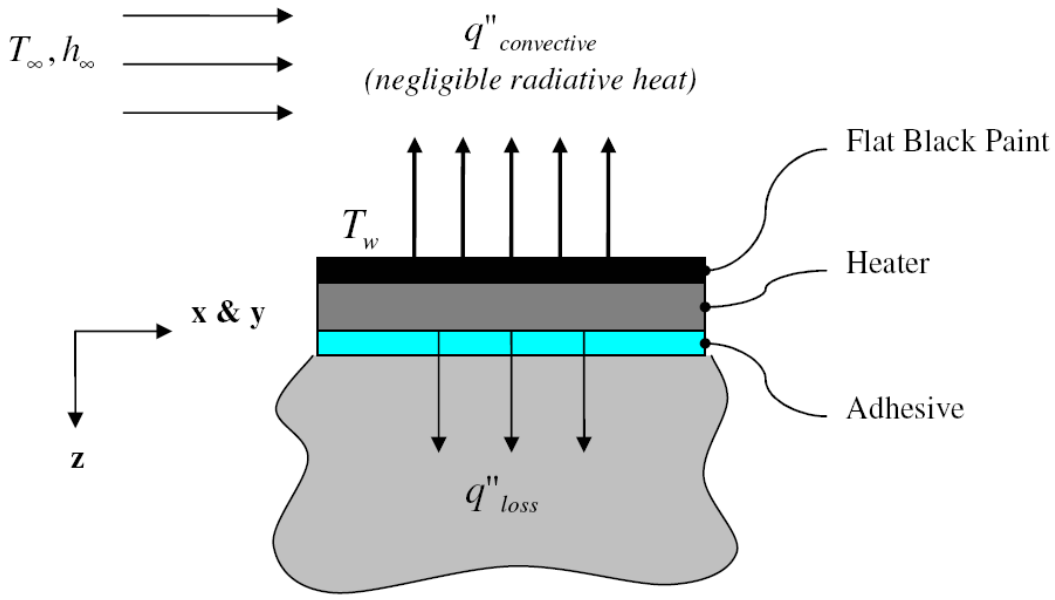

Fig 2.8: Schematic of the Surface Heater [23]

The entire outside wall of the combustor liner model was insulated using a thick layer of fiberglass insulations. However, a small amount of heat loss from the heater, by conduction into the liner wall and by radiation to the surroundings was unavoidable. The amount of heat loss is a function of the temperature of the combustor liner wall. During the experiment, the temperature along the liner wall varies. The temperature is lower closer to the swirler where high convective heat transfer occurs and is higher further away from the swirler. Therefore, the heat loss occurring along the liner wall at varying temperature regions needs to be evaluated. In order to establish this loss, the liner wall was heated without supplying air into the combustor model. Thereby all the heat energy is dissipated by conduction and radiation and not by forced convection. In other words the heat energy dissipated in this case will be the heat loss when air is blown through the combustor. This heat loss is measured at different temperatures so as to evaluate the heat loss at varying temperatures along the liner wall. The heat loss occurring at varying temperatures is plotted below.

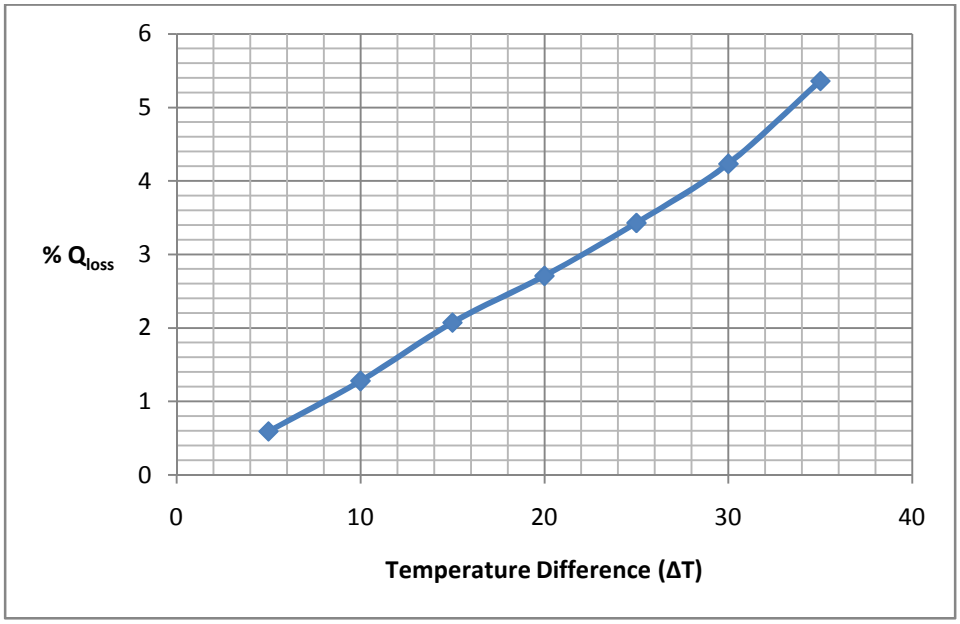

Figure 2.9: Heat loss from the liner wall as a function of temperature

Fig 2.10 shows the IR image of the heater when it is heated and the temperature distribution along its length can be observed.

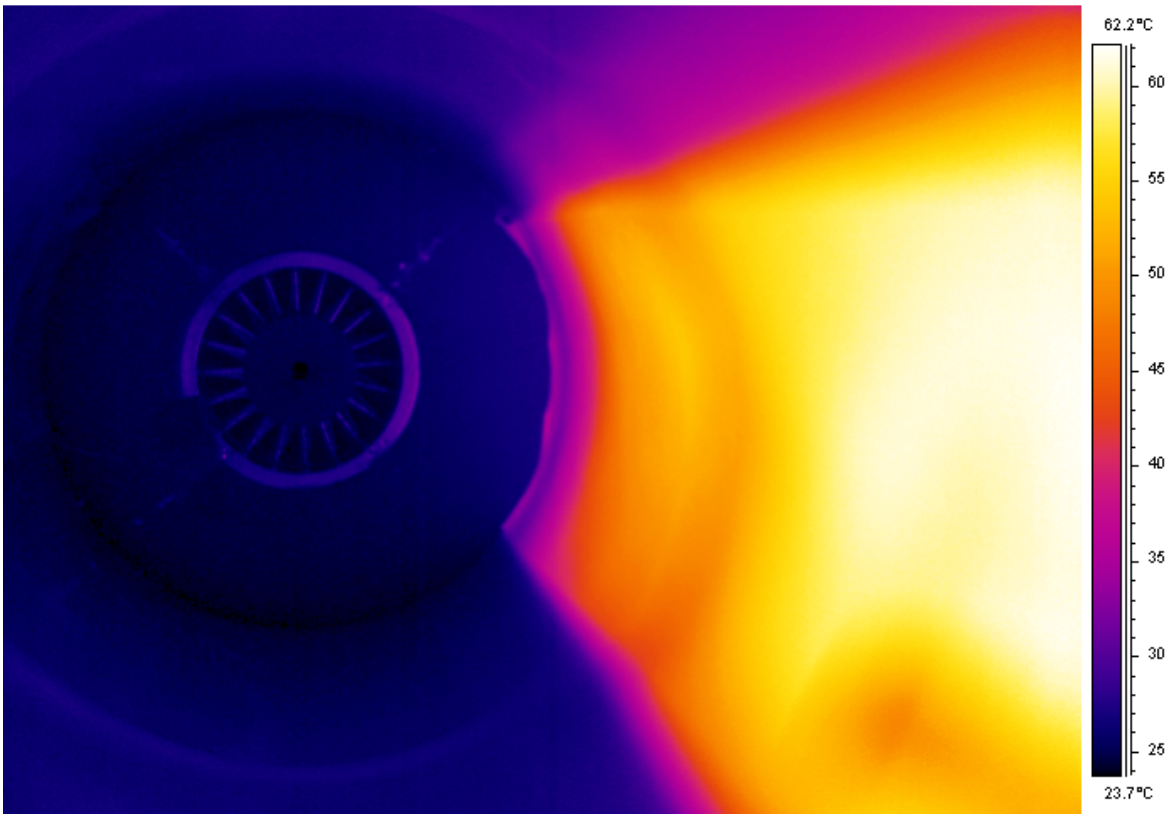

Figure 2.10: IR image of the surface heater on the liner wall (Photo by Author)

2.2.5 Infrared Thermal Imaging System

The FLIR SC640 Infrared Camera, shown in Figure 2.11 was used to capture the liner wall surface temperature distribution within the combustor. The SC640 camera is a focal plane array system type IR camera, using microbolometer as detector material and has thermal

sensitivity within 0.1ºC at 30ºC. The camera has a maximum resolution of 640x480 and wide measurement range of -40°C to +1,500°C, in 3 ranges. With proper calibration temperatures up to + 2000°C can be recorded. The target surface emissivity can be precisely calibrated and its emissivity can be adjustment from 0.1 to 1.00. The refresh frequency of imaging can be set to as fast as up to 60Hz. Thermography is the production of temperature calibrated infrared or heat pictures by utilizing an infrared camera. Based on these thermal images, accurate temperature measurements can be made to detect even the smallest temperature differences. It is not always possible to know where to attach the thermocouples necessary to make accurate measurements and effectively evaluate heat dissipation. Furthermore, since the thermocouple needs to be in contact with the component to be tested, it can influence the results of the measurement

Figure 2.11: FLIR SC640 Infrared Camera (Photo by Author)

. The ThermaCAM SC640 has the advantage that it produces very comprehensive images in a non-contact mode. It can produce very high resolution images (640 x 480 pixels) so that crisp thermal images can be taken of even the smallest of objects in a non-contact mode. The

camera is especially designed for the most demanding scientific applications and detects the smallest temperature differences over a very wide temperature range. Frames can be captured, and stored, in real-time, at high frame rates allowing for detailed and extensive analysis of highly dynamic events typically found in R&D environments.

2.2.6 Personal Daq USB Data Acquisition Module

Various thermocouples were positioned to obtain temperature values at the inlet to the combustor and also to calibrate the IR camera. The OMB-DAQ-54 Personal Daq, as shown in Fig 2.12 was used to acquire the thermocouples process signals. It is a full-featured data acquisition product that uses the Universal Serial Bus (USB) built into almost every new PC. Designed for high accuracy and resolution, the OMB-DAQ-54 data acquisition systems directly measure multiple channels of voltage, thermocouple, pulse, frequency, and digital I/O. A single cable to the PC provides high-speed operation and power to the OMB-DAQ-54. No additional batteries or power supplies are required, except when using bus-powered hubs. Because of the strict power limitations of the USB, the modules incorporate special power management circuitry to ensure adherence to USB specifications. The OMB-DAQ-54 module avoids many of the limitations of PC-card (PCMCIA) data acquisition devices and offer advantages over many PC plug-in data acquisition boards as well. The OMB-DAQ-54 data acquisition system offers 10 single-ended or 5 differential analog (up to ±20 V full scale) or thermocouple input channels with 16 programmable ranges and 500 V optical isolation. Two type K thermocouples were positioned at the inlet to the combustor to estimate the inlet temperature values. One cement-on

thermocouple was positioned on the combustor wall opposite one of the IR windows to calibrate the IR camera.

Figure 2.12: OMB-DAQ-54 Personal Daq (Photo by Author)

2.2.7 NetScanner 9816/98RK Ethernet Intelligent Pressure Scanner

The NetScanner System is a multi-channel pressure acquisition system. The system is comprised of a Model 98RK Scanner Interface Rack, housing up to eight Model 9816 Intelligent Pressure Scanners networked via the Ethernet interface. NetScanner System Intelligent Pressure Scanner modules are flexible pressure measuring devices intended for use in research and production environments. A single model 9816 Intelligent Pressure Scanner is available with sixteen measurement channels, each with individual pneumatic transducers per channel. During the experiments three of these scanners were used, totaling to 3 x 16 = 48 channels. The experimental combustor chamber consisted of 96 pressure taps along the liner wall as shown in figure 2.7.

Model 9816 pressure scanners are capable of accuracies up to ±0.05%. Accuracy is maintained through use of built-in re-zero and span calibration capabilities. 98RK Scanner Interface Rack features pneumatic hook-ups on the back-panel or front-panel (if ordered) to ease calibration of the scanners. Each 9816 Intelligent Pressure Scanner module contains a pneumatic calibration manifold and software commands to automatically perform re-zero and span adjustment calibrations. The 98RK chassis requires an 80 psig minimum dry air (or inert gas) supply which is used to shift the 9816 internal calibration valve (in each scanner) between its different positions. Each internal Model 9816 pressure scanner module (mounted in 98RK chassis slots) has an Ethernet interface to communicate with a host computer.

Figure 2.13: NetScanner multi-channel pressure acquisition system (Photo by Author)

CHAPTER 3: EXPERIMENTAL METHODOLOGY

The core combustion temperature at real engine conditions can get as high as 1850K, which is around the melting temperature of materials of typical turbine components without thermal barrier coating. The operating pressure within a combustor can be around 20 atm to 30 atm. It is not feasible to perform the experiment at these engine conditions due to factors such as cost effectiveness, available facilities and safety issues. Therefore, a non-reactive combustion investigation was considered as a more realistic and feasible option for this project. The intake air temperature was at room temperature and the operating pressure was the local atmospheric pressure. The experiments were conducted at two Reynolds numbers (50,000 and 80,000). To correlate the experimental results to real time engine condition values, it is imperative to conduct similarity analysis to establish the relationship between actual heat transfer coefficient and test model heat transfer coefficient. The experimental apparatus was set up on a one to one scale.

Real Engine Conditions:	Test Model Conditions:
Air Temp. =1850K	Air Temp. = 293K
k_{air}@1850 = 0.124 W/m K	k_{air}@293 = 0.0263W/m K
Operating pressure ~ 20 atm	Operating pressure ~ 1 atm

Similarity Analysis:

$$(Nu)_{\text{actual}} = (Nu)_{\text{test}}$$

$$\left(\frac{hD}{k}\right)_{\text{actual}} = \left(\frac{hD}{k}\right)_{\text{test}}$$

$$h_{actual} = \left(\frac{k_{actual}}{k_{test}}\right)\left(\frac{D_{test}}{D_{actual}}\right) h_{test} = 4.71 \text{ x } 1 \text{ x } h_{test} = 4.71\ h_{test}$$

Therefore, it is evident that the actual heat transfer coefficient at real engine condition should be about 4.71 times higher than the experimental results. It is imperative to conduct similarity analysis so that the experimental results can be utilized to validate the real engine operation investigation.

3.1 Transient Heat Transfer Measurement

During the first stage of this project conducted at Louisiana State University, a transient method was used to determine local heat transfer coefficients. A uniform initial wall temperature was applied on the combustor wall using surface wall heaters after which cold mainstream air was suddenly sent into the combustor chamber through the swirler. The following description will explain the model used to determine the heat transfer coefficient. The governing equations, boundary conditions, assumptions made and methodology used to solve the problem is described. Consider flow over an infinitely thick plate as depicted.

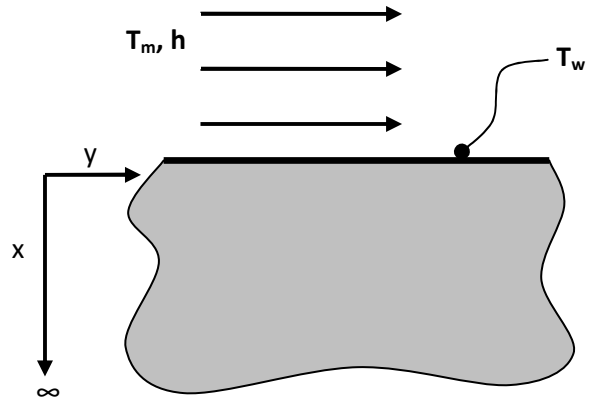

Fig 3.1: Flow over an infinitely thick plate [23]

In the transient case, the heated wall temperature at the first instance that the mainstream air, at room temperature, is passed through the chamber is recorded by the IR camera (T_i). For all time t > 0, the wall temperature will decrease as a response to the mainstream air passing over the liner wall, which is maintained at a constant heat flux. Equation 1 is the result of a thermal energy balance of the wall for t > 0, where T is the local wall temperature and α is the thermal diffusivity of the wall.

$$\left(\frac{\partial^2 T}{\partial x^2}+\frac{\partial^2 T}{\partial y^2}\right)=\frac{1}{\alpha}\frac{\partial T}{\partial t} \qquad (1)$$

Lateral conduction in the wall can be neglected and only conduction into the wall is considered, Equation 1 therefore reduces to Equation 2.

$$\frac{\partial^2 T}{\partial x^2}=\frac{1}{\alpha}\frac{\partial T}{\partial t} \qquad (2)$$

To solve this second order partial differential equation, an initial condition, and two boundary conditions are necessary. Equation 3 gives the initial condition for the temperature of the wall at t = 0. The two boundary conditions at x = 0 and infinity are given in Equations 4 and 5.

$$T = T_i \; at \; t = 0 \qquad (3)$$

$$-k\frac{\partial T}{\partial x} = h\left(T_w - T_m\right) \;\; at \; x = 0 \; and \; t \geq 0 \qquad (4)$$

$$T = T_i \; at \; x = \infty \; and \; t \geq 0 \qquad (5)$$

Solving the partial differential equation with the obtained initial and boundary conditions, at the point x = 0, gives the transient wall temperature response due to the convective heat flux leaving the wall for all time. The solution is given in Equation 6.

$$\frac{T_w - T_i}{T_m - T_i} = 1 - \exp\left(\frac{h^2 \alpha t}{k^2}\right) erfc\left(\frac{h\sqrt{\alpha t}}{k}\right) \quad (6)$$

Where,

T_w = Combustor liner wall temperature

T_i = Combustor liner initial temperature

T_m = Mainstream air temperature

k = Thermal conductivity of the wall

α = Thermal diffusivity of the wall

t = Time for which the measurements were taken

h = Heat transfer coefficient

In the above equation, all the physical properties are known. Thus by recording T_w at different time t, the value of heat transfer coefficient h can be determined. T_w values were obtained using the IR camera and were post processed using MATLAB to calculate the heat transfer coefficient values.

3.2 Steady-State Heat Transfer Measurement

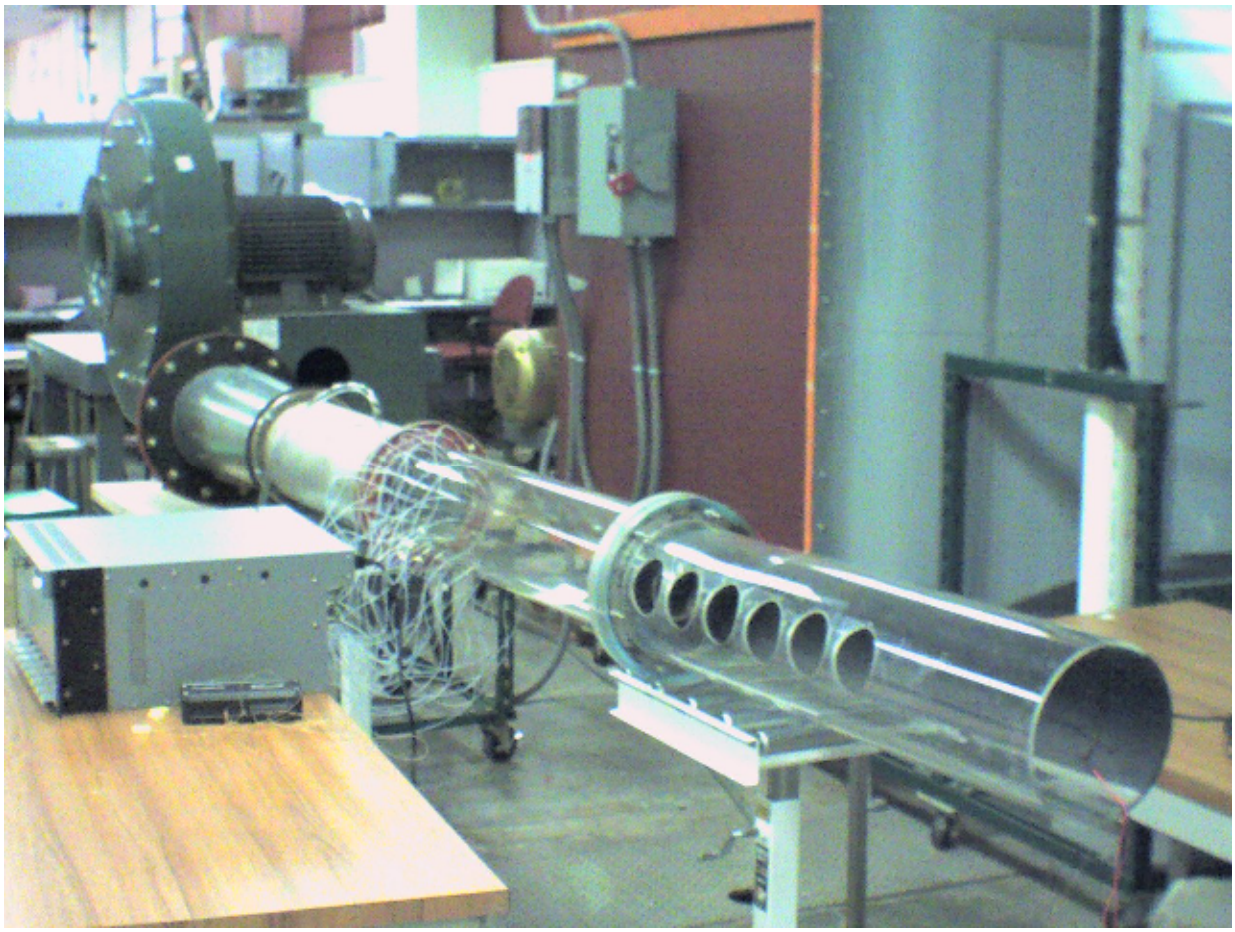

Fig 3.2: Steady-State experiment setup (Photo by Author)

The second stage of this project was conducted at the lab facilities in Virginia Polytechnic Institute and State University. Air at room temperature from the blower was sent into the main combustion chamber through the swirler mounted concentrically within the inlet chamber. The liner wall section diametrically opposite the IR window was heated uniformly with two identical surface heaters to simulate constant heat flux boundary condition. The heaters were connected in series across the length of the combustion chamber. The heat flux was adjusted using two variable transformers to obtain the desired temperature difference between the wall

and the bulk air. The inlet upstream and exit downstream air temperatures were measured with high sensitivity fine gauge K-type thermocouples using the OMB-DAQ-54 Personal Daq USB Data Acquisition Module temperature measuring system. Thermocouples were also used to calibrate the IR camera to ensure accurate measurements. A cement-on thermocouple was placed at a location on the combustor model liner and the IR camera was focused onto the exact same location. The emissivity settings on the IR camera was set to a value at which the temperature values obtained from the IR camera matched with the temperature values obtained from the thermocouple. The blower air supply system was switched on and set to the desired air flow rate using the adjustable frequency AC drive in order to obtain the required Reynolds numbers. Once the air flow speed was properly set, surface heaters were set to the required heat flux power to obtain the desired temperature values. Since the experiment was to be performed under steady-state method, the entire set up was left running for at least half an hour until a steady-state wall surface temperature is reached. The entire combustor chamber was covered with insulating material to prevent losses. The IR image of temperature distribution was acquired at six different locations along the combustion chamber. The raw temperature data from all six different images were merged and combined to compute the local heat transfer coefficient distributions. The basic convective heat transfer equation was used as shown below:

$$h = \frac{Q}{A(T_{wall} - T_{air})}$$

The heat flux was calculated using the resistance ratings of the heater and the voltage settings on the transformer. $Q = \frac{V^2}{R}$

The target surface emissivity was calibrated using an OMEGA cement-on thermocouple and the OMB-DAQ-54 Personal Daq Data Acquisition system temperature measuring system and was determined to be 0.92.

The combustor chamber was replaced with another one with 96 pressure taps, in order to obtain the pressure distribution. 12 pressure taps were drilled along half the circumference of the chamber at 8 different locations along the axial distance and the static pressure values were detected using the NetScanner System, a multi-channel pressure acquisition. The static pressure value prior to the swirler inlet was also obtained.

3.3 Uncertainty Analysis

In order to determine the accuracy of this study, an error analysis is preformed using the methodology of Kline and McClintock. First, a conservative error estimate of the measured quantities was determined and then the relative uncertainties in measured quantities were calculated. Finally, the overall average uncertainty was calculated by taking the square root of the summation of the square of all the relative uncertainties.

3.3.1 Transient condition experiment uncertainty analysis

Heat transfer coefficient for flow in the combustor model was calculated using the following equation

$$\frac{T_w - T_i}{T_m - T_i} = 1 - \exp\left(\frac{h^2 \alpha t}{k^2}\right) erfc\left(\frac{h\sqrt{\alpha t}}{k}\right)$$

Thus, $h = f(T_w, T_i, T_m, \alpha, k, t)$

Error estimates of each variable are as follows

The wires used in OMEGA thermocouples are selected and matched to meet ANSI limits of Error.

$\Delta T_w = 0.5^oC$

$\Delta T_i = 0.5^oC$

$\Delta T_m = 0.5^oC$

$\Delta t = 1$ seconds

Here, α and k are tabulated values. As a practice, three percent relative uncertainty is assumed for both variables.

$U_\alpha = U_k = 0.03$

The relative uncertainties of the rest of the four variables are given by:

$U_{Tw} = \Delta T_w / T_w$

$U_{Ti} = \Delta T_i / T_i$

$U_{Tm} = \Delta T_m / T_m$

$U_t = \Delta t / t$

The root mean square uncertainty in calculating heat transfer coefficient:

$\mathbf{U_h} = \{(U_{Tw})^2 + (U_{T\,i})^2 + (U_{T\,m})^2 + (U_t)^2 + (U_\alpha)^2 + (U_k)^2\}^{½} = \mathbf{\pm 5.1\%}$

Therefore, the overall average uncertainty in h during the transient technique was estimated to be ± 5.1%

3.3.2 Steady-State condition experiment uncertainty analysis

The heat input was calculated using the resistance ratings of the heater and the voltage settings on the transformer. $Q = \frac{V^2}{R}$

Error estimates of each variable are as follows

$\Delta R = 0.45\ \Omega$ (obtained from the ratings for the heater)

$\Delta V = 2$ V (LC of the variable transformer used to set the voltage during the experiment)

The relative uncertainties of the variables are

$U_R = \Delta R/R$

$U_V = \Delta V/V$

The root mean square uncertainty in calculating heat input:

$U_Q = \{(2U_V)^2 + (U_R)^2\}^{1/2} = \pm 5.1\%$

Heat transfer coefficient for flow in the combustor model was calculated using the following equation

$$h = \frac{Q}{A(T_{wall} - T_{air})}$$

Error estimates of each variable are as follows

A=B*L

$\Delta B = 0.0625$ inches (LC of the measuring tape used)

$\Delta L = 0.0625$ inches

$\Delta T_{wall} = 0.5^oC$

$\Delta T_{air} = 0.5^oC$

The relative uncertainties of the variables are

$U_Q = \pm 5.1\%$

$U_L = \Delta L/L$

$U_B = \Delta B/B$

$U_{Twall} = \Delta T_{wall}/T_{wall}$

$U_{Tair} = \Delta T_{air}/T_{air}$

The root mean square uncertainty in calculating the heat transfer coefficient:

$\mathbf{U_h} = \{(U_Q)^2 + (U_B)^2 + (U_L)^2 + (U_{Twall})^2 + (U_{Tair})^2\}^{½} = \mathbf{\pm 5.7\%}$

Therefore, the overall average uncertainty in h during the steady state experiment was estimated to be ± 5.7%

Uncertainty in Reynolds Number:

$Re = (V * D) / \nu$

Error estimates of each variable are as follows

ΔV= 0.1 m/s (LC of the Pitot tube measurements)

ΔD = 0.0625 inches

The relative uncertainties of the variables are

$U_V = \Delta V/V$

$U_D = \Delta D/D$

Here, ν is a tabulated value. As a practice, three percent relative uncertainty is assumed.

$U_\nu = 0.03$

The root mean square uncertainty in calculating the Reynolds number:

$U_{Re} = \{(U_V)^2 + (U_D)^2 + (U_\nu)^2\}^{½} = \mathbf{\pm 4.0\%}$

Therefore, the overall average uncertainty in Re was estimated to be ± 4.0%

Uncertainty in Nusselt Number:

$Nu = (h * D) / k$

Error estimates of each variable are as follows

ΔD = 0.0625 inches

The relative uncertainties of the variables are

$U_D = \Delta D/D$

$U_k = 0.03$ (As a custom, three percent relative uncertainty is assumed)

$U_h = 5.7\%$ for steady-state and 5.1% for transient technique experiment

The root mean square uncertainty in calculating the Nusselt number:

$U_{Nu} = \{(U_h)^2 + (U_D)^2 + (U_k)^2\}^{½}$

$U_{Nu} = \pm 6.4$ % for steady-state

$U_{Nu} = \pm 5.9\%$ for transient

Therefore, the overall average uncertainty in Nu during the steady state experiment was estimated to be ± 6.4% and for the transient technique experiment was ± 5.9%

CHAPTER 4: RESULTS

4.1 Transient condition experiment: Heat transfer data

The transient condition experiment was run by maintaining the pressure in the combustor region at 3.5% above atmospheric pressure using a pneumatic valve placed upstream of the combustor chamber. Air is sent into this pneumatic valve from a high volume compressor. The Reynolds number corresponding to this condition was recorded as 50,000. The IR camera measured the surface temperature of the combustor liner model. The temperature values were then used in a MATLAB program to calculate the heat transfer coefficient values. Thermocouples placed downstream of the swirler provided the ambient intake air temperature. The constant heat flux was calculated by using the resistance ratings of the wall heater and the output voltage set on the transformer. The obtained power (wattage) was then divided by the area of the heater to obtain the constant heat flux value.

In order to conduct non dimensional analysis, Nusselt number comparison was done. To determine the augmentation in Nusselt number values we need to compare it with the developed straight pipe channel estimation of heat load and flow characteristics, also known as Dittus-Boelter Equation, which is the current design criterion of cooling systems used within combustors. The Dittus-Boelter equation (for turbulent flow) is an explicit function for calculating the Nusselt number. It is easy to solve but is less accurate when there is a large temperature difference across the fluid. The Dittus-Boelter equation is:

$$Nu_{fd} = 0.023 Re_D^{0.8} Pr^{0.3}.$$

Fig 4.1 shows the Nu/Nu_{fd} augmentation values. This is basically the ratio of the experimental results to the fully developed straight pipe estimation of the local heat load distribution. Due to the fact that the experiment was of a transient nature and was conducted in a blow down facility, every time the IR camera was moved to a different location along the combustor model liner, the experiment was rerun. Therefore each image that was captured and processed was obtained from a different run, but at the exact same conditions. However, complete repeatability could not be achieved for each run. This is the reason that the missteps are seen in the graph. The uncertainty could not be estimated due to fluctuating flow during the multiple runs, occurring due to irregularity in the control valve settings of the pneumatic valve. In order to ensure more reliable results, it was decided that steady state experiments needed to be conducted. Due to the fact that a correct error estimate could not be evaluated, the results obtained from the transient condition experiment are not used in the further analysis of this research study. However, the overall trend from the transient experiment is similar to the steady state results (shown in the next section).

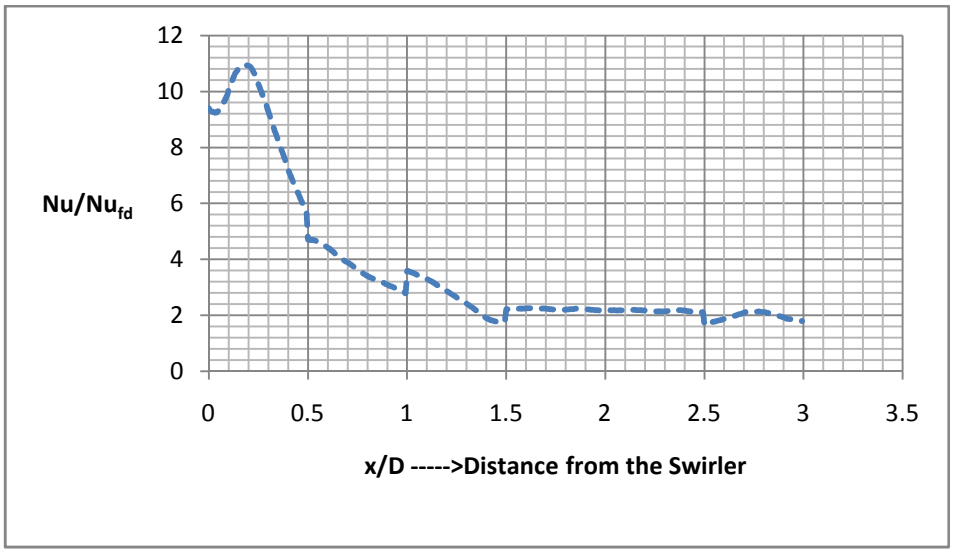

Fig 4.1: Local Nusselt Number Augmentation with respect to fully developed straight pipe values at Re=50,000

4.2 Steady-State condition experiment: Heat transfer data

The steady-state condition experiment was conducted by blowing air from a blower programmed by an adjustable frequency AC drive to obtain Reynolds numbers of ~ 50,000 and ~ 80,000. The IR camera measured the surface temperature of the combustor. Post processing of the temperature data was done using MATLAB to obtain the heat transfer coefficient values.

Figure 4.2 shows the 2-D temperature distribution map along the length and width of the liner wall. The swirler at the entrance of the combustor causes the flow to swerve sharply from its original direction due to the high angle of swirl, thus impinging on the liner wall upstream very close to the swirler. It can therefore be seen that the temperature downstream remains much higher than that upstream. From the picture, slightly higher temperatures can be seen at the center of the wall. This is because of slight losses from the edges of the heater. To reduce the effect of these losses, during post processing, only the central 50% of the wall temperature is used to calculate the heat transfer coefficient.

Re = 50,000

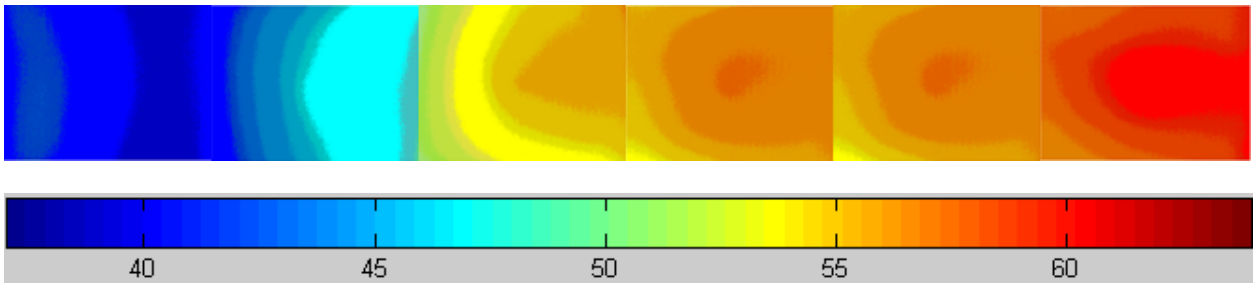

Fig 4.2: 2-D temperature distribution (in °C) along length and width of the liner wall for Re=50,000and Re=80,000

Re = 80,000

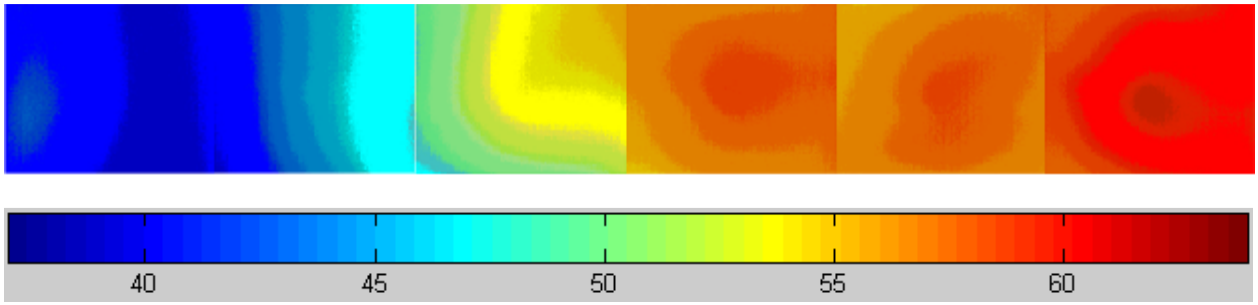

Fig 4.2: 2-D temperature distribution (in °C) along length and width of the liner wall for Re=50,000and Re=80,000

Fig 4.3 shows the 2-D heat transfer rate distribution map along the liner wall. It can be seen that the heat transfer rate is higher upstream and lower downstream from the swirler. There is clearly a distinguishable localized heat transfer peak region within the combustor.

Re = 50,000

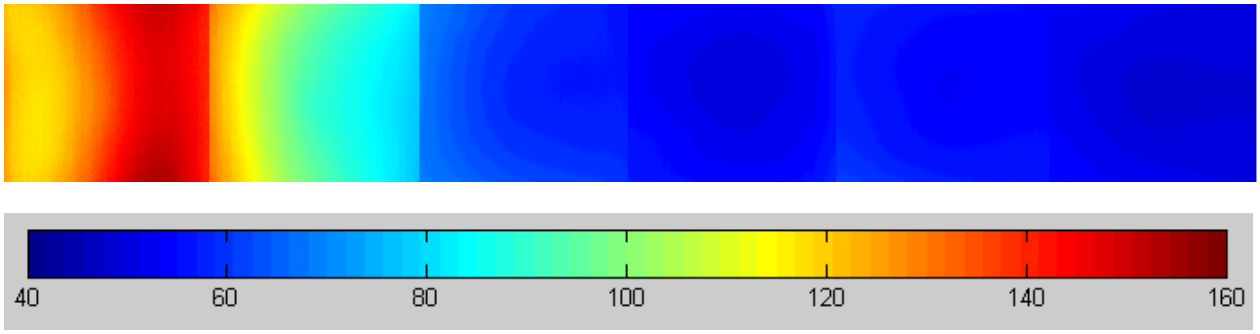

Re = 80,000

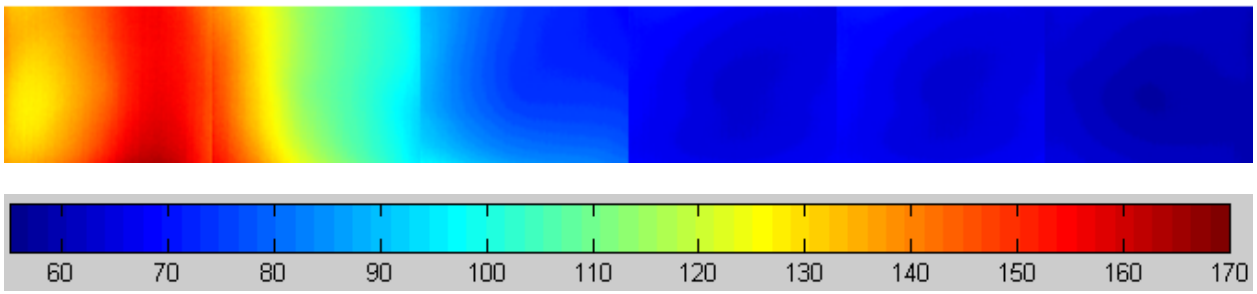

Fig 4.3: 2-D heat transfer distribution (in W/m^2K) along the liner wall for Re=50,000 and Re=80,000

Figure 4.4 illustrates a 1-D profile of the heat transfer distribution along the length of the combustor liner wall. From the curve an evident peak can be seen which represents a region of positive local hot spot on the real engine combustor liner, pertaining to the highest heat transfer coefficient and concentrated heat load. It can also be seen that there is a decrease in heat transfer as the distance from the swirler increases after the high heat transfer region is reached. The heat transfer peak value for Re=50,000 is about 150W/m^2K and for Re=80,000 is about 160W/m^2K.

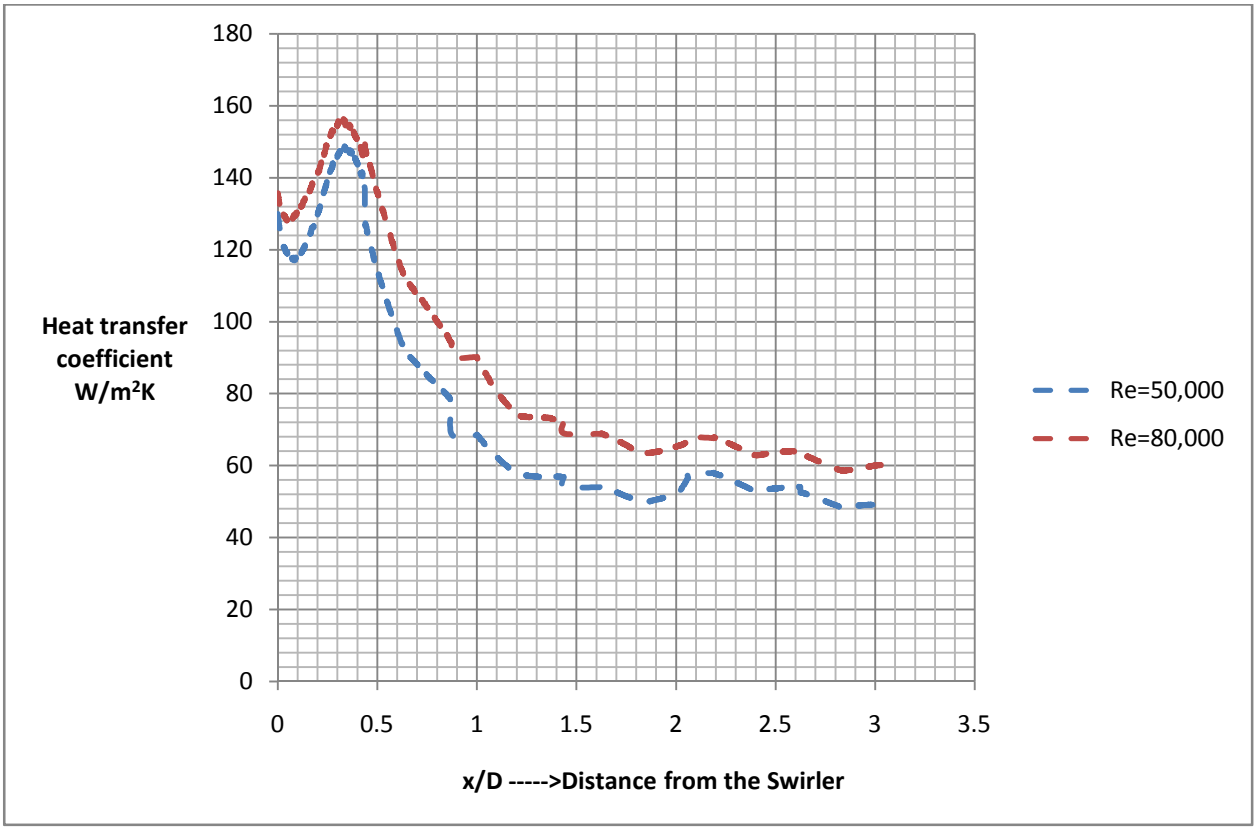

Fig 4.4: 1-D heat transfer coefficient distribution along the liner wall for Re=50,000 and Re=80,000

For further analysis the non dimensional number, Nusselt number was used. As done previously for the transient state experiment, to determine the augmentation in Nusselt number values, we compare it with the developed straight pipe channel estimation of heat load, also

known as Dittus-Boelter Equation. Fig 4.5 displays the local Nusselt number variations with reference to combustor diameter for both Re=50,000 and Re=80,000.

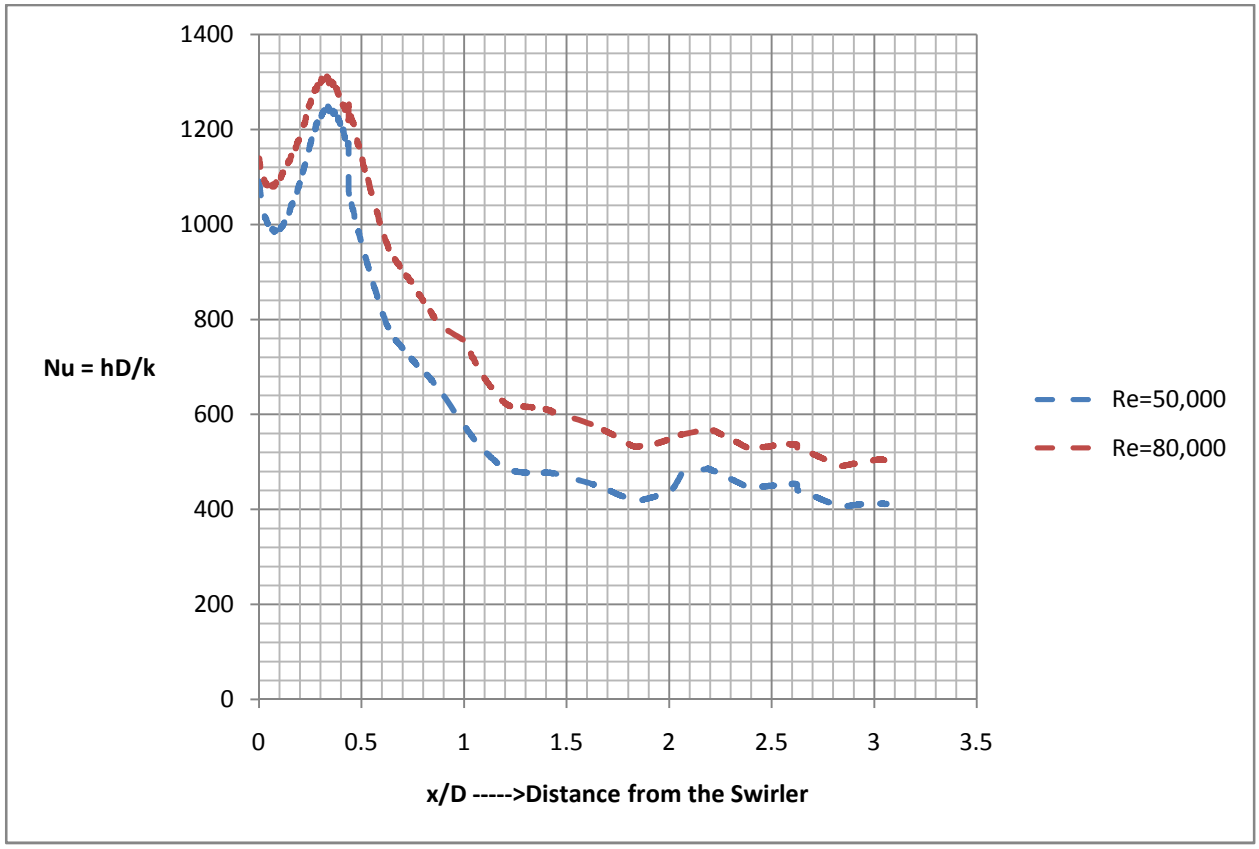

Fig 4.5: Nusselt number variations with reference to combustor diameter for both Re=50,000 and Re=80,000

The Dittus-Boelter equation is: $Nu_{fd} = 0.023 Re_D^{0.8} Pr^{0.3}$.

Fig 4.6 shows the Nu/Nu_{fd} augmentation values. This is basically the ratio of the experimental results to the fully developed straight pipe estimation of the local heat load distribution.

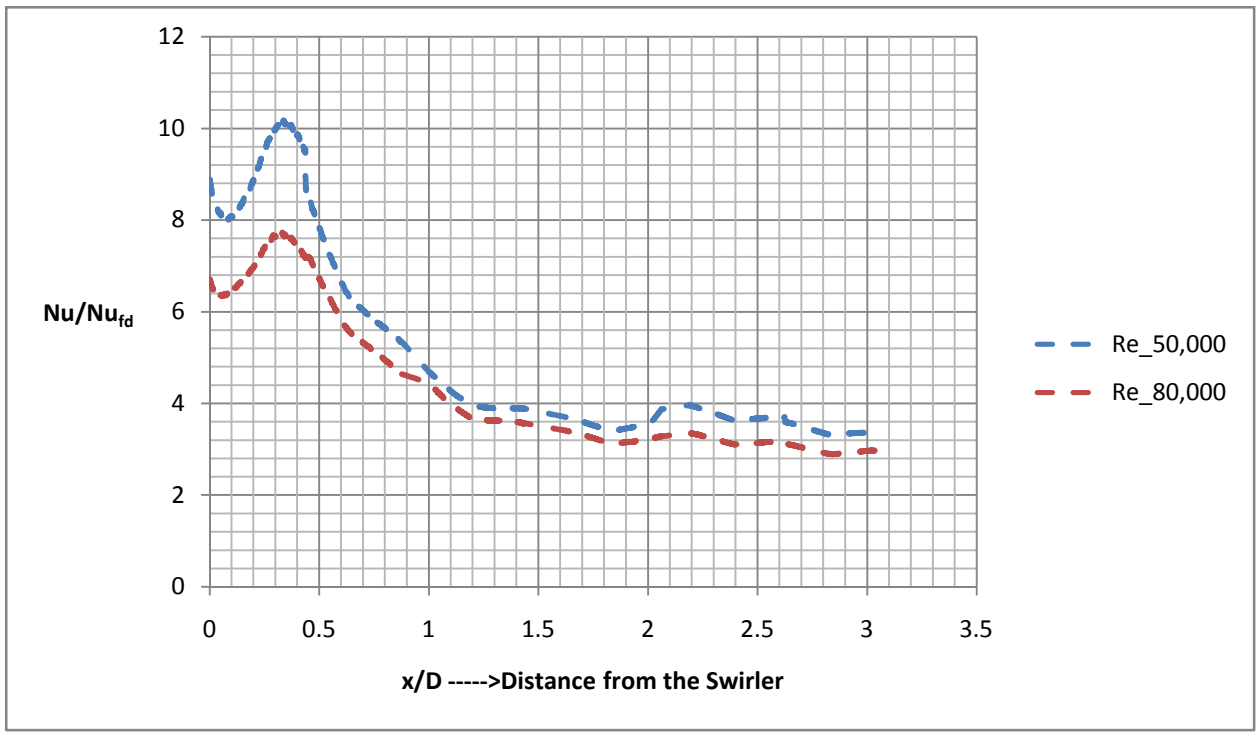

Fig 4.6: Local Nusselt Number Augmentation with respect to fully developed straight pipe values at Re=50,000 and Re=80,000

From the above graph it is obvious that the lower Reynolds number (50,000) case shows a higher augmentation with respect to the fully developed straight pipe estimation than the higher Reynolds number (80,000) case does. Another important observation is that the location of maximum augmentation (peak heat transfer coefficient) along the liner wall is almost identical for both Reynolds number of 50000 and 80000. The curve trends are also identical. These results convince us that the Nusselt number distribution at any Reynolds number would have the same trend.

Previously, at Louisiana State University [23], experiments were conducted at higher Reynolds numbers. The actual test model was 5-times the original 8" (20.32cm) diameter prototype to simulate realistic engine operating conditions and also provide high resolution

measurements. Experiments were performed at two flow Reynolds Numbers (500,000 and 662,000) to further investigate the effects of Reynolds Number on the heat transfer peak locations and velocity flow field distributions. Figure 4.7 shows the ratio of the experimental results to the fully developed straight pipe estimation of the local heat load distribution.

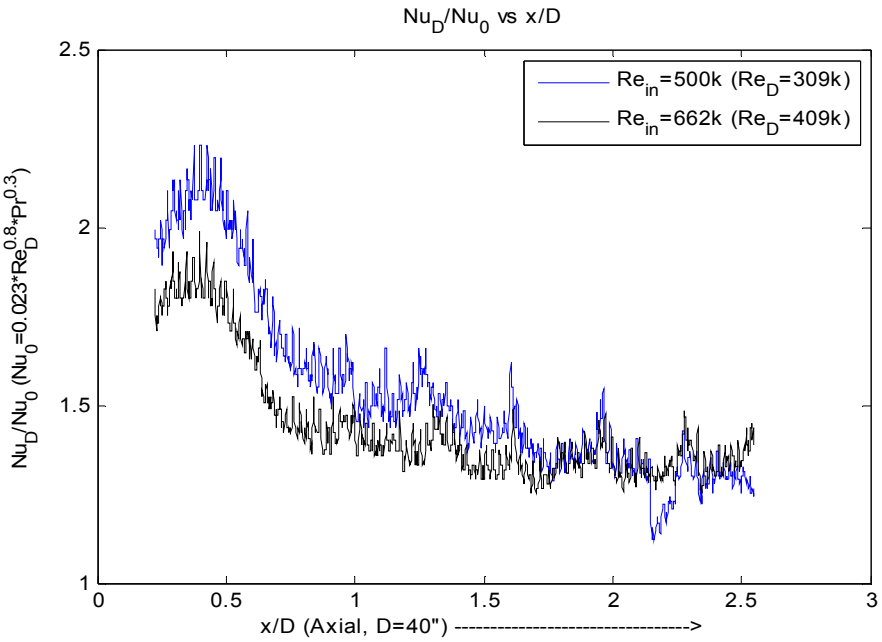

Figure 4.7: Comparison of Local Nusselt Number Distribution to FDF Straight-pipe Estimation for Re=500,000 and 662,000 [23]

Comparing all the results, it appears that the overall augmentation levels are decreasing as axial flow velocity (as in Reynolds number) increases. This may be primarily because of the increased mean velocity in relation to the turbulence production due to the induced swirling. This reduces the local turbulence production and thus reduces the local turbulence intensity that impacts the wall surfaces and causes enhanced heat transfer. The turbulence intensity due to swirl is the prime impact on the surface heat transfer coefficient. It is clear that increased Reynolds number thus produces lower heat transfer coefficients due to reduce local turbulence intensity.

4.3: Validation with CFD Results

CFD analysis was conducted at Virginia Polytechnic Institute and State University by Sunil Patil under the guidance of Dr. Danesh Tafti. The location of peak heat transfer region remains nearly same for both Reynolds number. The maximum Nusselt number augmentation value for Re 50000 is around 10.5 while it reduces to about 8 for Re 80000. Different RANS based turbulence models were tested to determine the ability of these models to predict the swirling flow. RNG k-ε model predicts the location of the peak heat transfer location with very close Nusselt number augmentation value at that region as obtained through experimental study. There exists a strong recirculation region in the upstream corner region in combustor for both cases.

It was found out that the RNG k-ε with swirl modifications works better in predicting the location of peak heat transfer and Nusselt number augmentation value than standard k-ε, realizable k-ε and SST (Shear Stress Transport) k-ω.

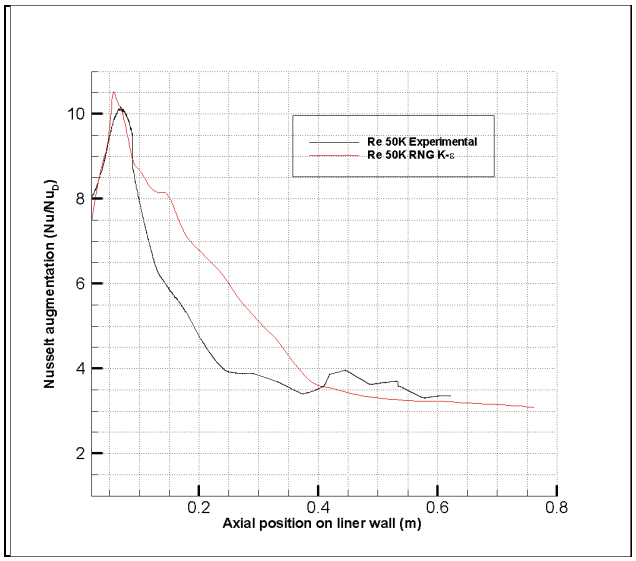

Fig 4.8: Nusselt number Augmentation for Re = 50000 (CFD)

4.4 Effect of Reynolds number on Nusselt number augmentation

The peak values obtained from the experiments and CFD analysis are plotted as shown in Figure 4.9 below, in an effort to study the effect of Reynolds number on Nusselt number augmentation. It can be seen that as the Reynolds number goes higher, the peak Nusselt number augmentation value reduces. For real time engine conditions, the Reynolds number is around 300,000. From the graph, the Nusselt number augmentation values at Re ~ 300,000 are in the range of 4-5 and follow from the measurements done at low as well as high Reynolds numbers.

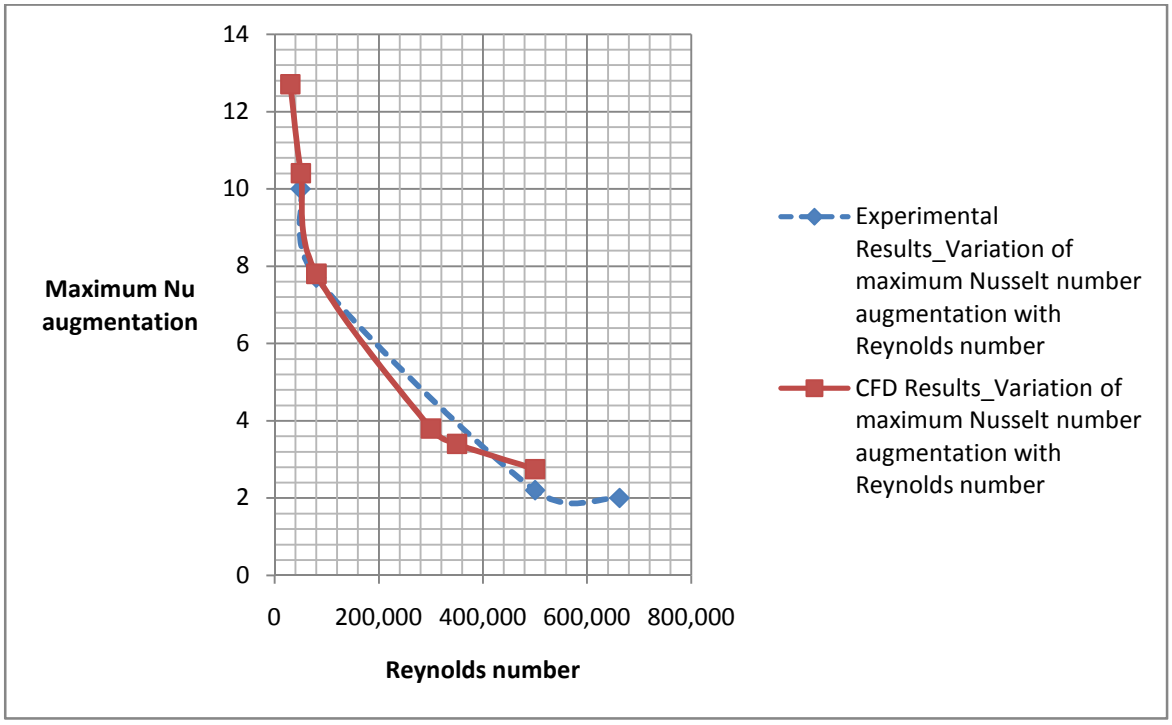

Fig. 4.9: Variation of Peak Nusselt number augmentation with Reynolds number

4.5 Steady-State condition experiment pressure data

Pressure data was obtained at 96 locations along the length and circumference of the liner (P_s). Fig 4.10 shows the circumferential averaged pressure distribution along the axial distance. It

is evident that there is a striking similarity between the pressure distribution and the heat transfer distribution. Analogous to the heat transfer distribution, we can see the pressure distribution increase slightly downstream of the swirler and then reducing down to a much lower value. The static pressure values measured at a location prior to the swirler entrance (P_{in}) were 0.16 psig and 0.40 psig for Re 50,000 and Re 80,000 respectively. The flow is redirected through the swirler and the high pressure region on the combustor model liner indicates the position of the first and highest impact of the incoming air. From the heat transfer results it can be seen that the region of highest heat transfer coefficient coincides with the region of highest static pressure, which makes sense. This clearly indicates the close relationship between the static pressure values and the heat transfer coefficient values on the combustor liner. Therefore the static pressure results validate the heat transfer results to a good extent. Fig 4.10 shows a graph of $\Delta P/P_{in}$ where $\Delta P = P_s - P_{in}$.

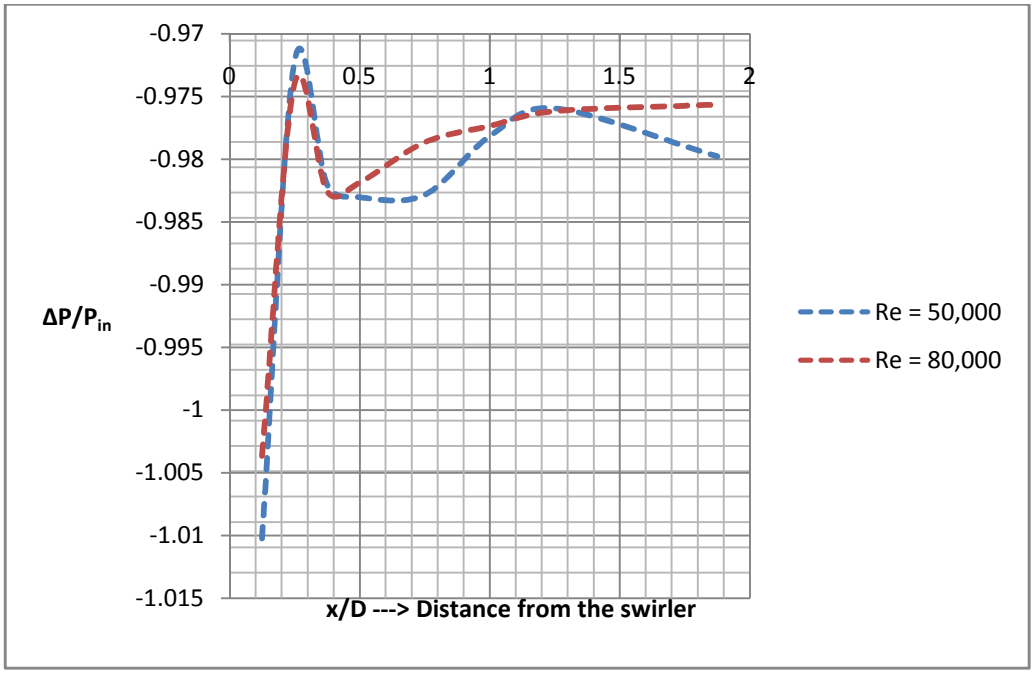

Fig 4.10: Pressure distribution along the liner wall

CHAPTER 5: CONCLUSIONS

The goal of this project was to study the heat transfer distribution and flow characteristics inside a "Dry Low NOx Emission" combustor model equipped with a swirler, provided by Solar Turbines, Inc., in order to better understand the flow behavior that effect the heat loads within a turbine combustor, to help design a more effective cooling system. The overall aim of this study is to provide a better understanding of the combustor swirling flow and its effect on liner surface heat transfer. Detailed heat transfer coefficient measurements on the liner wall at different Reynolds numbers using Infra-red thermography were presented.

The location of hot spots in a real engine (high heat transfer region in the experiment) was also determined for different Reynolds numbers to establish the concentrated heat load region, because the localized maximum heat load on the liner wall is a vital factor that has to be considered while designing a proper cooling system using focused back-side cooling technique.

Transient condition experiments as well as steady-state condition experiments were conducted at different Reynolds numbers. The peak locations of the heat transfer distribution were the same in both the cases. The Nusselt number augmentation values were also in agreement. The static pressure distribution data revealed that the peak location of the heat load and the peak location of the static pressure also matched. This is in a way a verification of the thermal results. The heat transfer and static pressure results prove and support each other to further compliment the findings. Another interesting find was that the peak location of the heat transfer coefficient (Nu), temperature and static pressure does not vary with the Reynolds number. The peak location for heat load and static pressure appeared at the same spot regardless of the flow rate and Reynolds number. This leads us to believe that a localized focused cooling

system can be designed safely, without giving a lot of thought about the variation in location with varying Reynolds number at real engine operation conditions. However, the effect that combustion has on the heat distribution on the liner has to be studied.

CFD analysis results were in good agreement with the experimental results. It was also found that the Nusselt number augmentation decreases as the Reynolds number goes higher. Results obtained from research experiments conducted previously for high Reynolds numbers (500,000 and 662,000) were compared with results obtained from this study at lower Reynolds numbers (50,000 and 80,000) in order to get a clearer picture of what the augmentation values are at real engine operation conditions (Re ~ 300,000). It is anticipated that this work will help improve design practices in combustor liner cooling for low emissions combustors.

References

1. Lefevebre, A. H., “Gas Turbine Combustion”, Taylor & Francis, 2nd Edition, 1998.
2. Alkabie, H., McMillan, R., Noden, R., Morris, C., 2000, “ Dual Fuel Dry Low Emission (DLE) Combustion System for the ABB ALSTOM Power 13.4MW Cyclone Gas Turbine, ASME paper 2000-GT-0111.
3. Peltier, R., “Gas turbine combustors drive emissions toward nil”, POWER, March 2003.
4. Bailey, J.C., Intile, J., Fric, T.F., Tolpadi, A.K., Nirmalan, N.V., Bunker, R.S., 2003, “Experimental and Numerical Study of Heat Transfer in a Gas Turbine Combustor Liner”, ASME J. Eng. for gas turbines and power, 03, pp. 994-1002.
5. Beer, J.M., and Chigier, N.A., “Combustion Aerodynamics”, Applied Science, London, 1972.
6. Kilik, E., “The influence of Swirler Design Parameters on the Aerodynamics of the Downstream Recirculation Region,” PhD thesis, School of Mechanical Engineering, Cranfield Institute of Technology, England, 1976.
7. Chin, J., Skirvin, S., Hayes, L., and Burggraf, F., 1961, ‘‘Film Cooling With Multiple Slots and Louvers—Part 1: Multiple Continuous Slots,’’ ASME J. Heat Transfer, 83, pp. 281–286.
8. Metzger, D. E., Takeuchi, D., and Kuenstler, P., 1973, ‘‘Effectiveness and Heat Transfer With Full-Coverage Film Cooling,’’ ASME J. Eng. Power, 95, pp. 180–184.
9. Andrews, G. E., Khalifa, I. M., Asere, A. A., and Bazdidi-Tehrani, F., 1995, ‘‘Full Coverage Effusion Film Cooling With Inclined Holes,’’ ASME Paper 95-GT-274.
10. Fric, T. F., Campbell, R. P., and Rettig, M. G., 1997, ‘‘Quantitative Visualization of Full-Coverage Discrete-Hole Film Cooling,’’ASME Paper 97-GT-328.

11. Schulz, A., 2001, ‘‘Combustor Liner Cooling Technology in Scope of Reduced Pollutant Formation and Rising Thermal Efficiencies,’’ *Heat Transfer in Gas Turbine Systems*, Ann. NY. Acad. Sci., 934, pp. 135–146.
12. Ferrara, G., Innocenti, L., Migliorini, G., Facchini, B., and Dean, A. J., 2000, ‘‘Heat Transfer Analysis in a Modern DLN Combustor,’’ ASME Paper 2000-GT-254.
13. Smith, K., and Fahme, A., 1999, ‘‘Backside Cooled Combustor Liner for Lean-Premixed Combustion,’’ ASME Paper 99-GT-239.
14. Smith, K.O., Angello, L.C., and Kurzynske, F.R., “Design and Testing of an Ultra- Low NOx Gas Turbine Combustor”, ASME Paper 86-GT-263, 1986.
15. Smith, K.O., Holsapple, A.C., Mak, H.H., and Watkins, L., “Development of a Natural Gas-Fired, Ultra-Low NOx Can Combustor for a 800kW Gas Turbine”, ASME Paper 91-GT-303, 1991.
16. Smith, K.O., and Cowell, L.H., “Experimental Evaluation of a Liquid Fuels, Lean Premixed Gas Turbine Combustor”, ASME Paper 89-GT-264, 1989.
17. Vandervort, C.L., “9 PPM NOx/CO Combustion System for “F” Class Industrial Gas Turbines”, ASME Paper 2000-GT-0086, 2000.
18. White, D.J., Batakis, A., Le Cren, R.T., and Yacabucci, H.G., “Low NOx Combustion Systems for Burning Heavy Residual Fuels and High Fuel-Bound Nitrogen Fuels”, J. Engg. Turbines Power, 104, 377-385, 1982.
19. Roberts, P.B., Kubasco, A.J., and Sekas, N.J., “Development of a Low NOx Lean Premixed Annular Combustor”, J. Engg. Turbines Power, 104, 28-35, 1982.
20. Arellano, L., Smith, K., and Fahme, A., “Combined Back Side Cooled Combustor Liner and Variable Geometry Injector Technology”, ASME Paper 2001 – GT – 0086, 2001.

21. Behrendt, T., Hassa, C., “A test rig for investigations of gas turbine combustor cooling concepts under realistic operating conditions”, J. Aerospace Eng., 222, 169-177, 2008.
22. Lu, Y.P., Esposito, E., Ekkad, S.V., “Predictions of flow and heat transfer in low mission combustors”, Heat Transfer Eng., 29, 375-384, 2008.
23. Goh, Y., “Heat transfer and flow characteristics inside a gas turbine combustor”, MS thesis, Department of Mechanical Engineering, Louisiana State University, 2006.
24. Image obtained from the sponsors by private correspondence with Dr. Srinath V. Ekkad (Committee chair)